AD

USAAMRDL TECHNICAL REPORT 69-33

STABILITY OF THIN-WALLED UNSTIFFENED CIRCULAR CYLINDRICAL SHELLS UNDER NONUNIFORMLY DISTRIBUTED AXIAL LOAD

By

W. H. Horton
J. W. Cox

November 1971

EUSTIS DIRECTORATE
U. S. ARMY AIR MOBILITY RESEARCH AND DEVELOPMENT LABORATORY
FORT EUSTIS, VIRGINIA

CONTRACT DA 44-177-AMC-258(T)
STANFORD UNIVERSITY
STANFORD, CALIFORNIA

DISCLAIMERS

The findings in this report are not to be construed as an official Department of the Army position unless so designated by other authorized documents.

When Government drawings, specifications, or other data are used for any purpose other than in connection with a definitely related Government procurement operation, the United States Government thereby incurs no responsibility nor any obligation whatsoever; and the fact that the Government may have formulated, furnished, or in any way supplied the said drawings, specifications, or other data is not to be regarded by implication or otherwise as in any manner licensing the holder or any other person or corporation, or conveying any rights or permission, to manufacture, use, or sell any patented invention that may in any way be related thereto.

Trade names cited in this report do not constitute an official endorsement or approval of the use of such commercial hardware or software.

DISPOSITION INSTRUCTIONS

Destroy this report when no longer needed. Do not return it to the originator.

DEPARTMENT OF THE ARMY
U. S. ARMY AIR MOBILITY RESEARCH & DEVELOPMENT LABORATORY
EUSTIS DIRECTORATE
FORT EUSTIS, VIRGINIA 23604

ERRATUM

USAAVLABS Technical Report 69-33
TITLE: Stability of Thin-Walled Unstiffened Circular Cylindrical Shells Under Nonuniformly Distributed Axial Load

Make the following pen and ink change on the cover:

USAAMRDL Technical Report 69-33 should read USAAVLABS Technical Report 69-33

Unclassified

Security Classification

DOCUMENT CONTROL DATA - R & D

(Security classification of title, body of abstract and indexing annotation must be entered when the overall report is classified)

1. ORIGINATING ACTIVITY (Corporate author) Stanford University Stanford, California	2a. REPORT SECURITY CLASSIFICATION Unclassified 2b. GROUP

3. REPORT TITLE
STABILITY OF THIN-WALLED UNSTIFFENED CIRCULAR CYLINDRICAL SHELLS UNDER NONUNIFORMLY DISTRIBUTED AXIAL LOAD

4. DESCRIPTIVE NOTES (Type of report and inclusive dates)

5. AUTHOR(S) (First name, middle initial, last name)
W. H. Horton
J. W. Cox

6. REPORT DATE	7a. TOTAL NO. OF PAGES	7b. NO. OF REFS
November 1971	87	13

8a. CONTRACT OR GRANT NO	9a. ORIGINATOR'S REPORT NUMBER(S)
DA 44-177-AMC-258(T) b. PROJECT NO. Task 1F162204A17001 c. d.	USAAVLABS Technical Report 69-33 9b. OTHER REPORT NO(S) (Any other numbers that may be assigned this report) SUDAER No. 220

10. DISTRIBUTION STATEMENT

Approved for public release; distribution unlimited.

11. SUPPLEMENTARY NOTES	12. SPONSORING MILITARY ACTIVITY
Supersedes AD-632921	Eustis Directorate, U. S. Army Air Mobility Research and Development Laboratory, Fort Eustis, Virginia

13. ABSTRACT

The report presents an experimental study of the stability of thin-walled circular cylindrical shells under nonuniformly distributed axial compression. Two techniques are given. The first is based on single tests of many specimens; the second, on many tests on a single specimen. The results are in excellent agreement. They demonstrate that such shells buckle when the stress at any point on their surface reaches the critical value for uniform axial compression.

DD FORM 1 NOV 68 1473

Unclassified

Security Classification

14. KEY WORDS	LINK A		LINK B		LINK C	
	ROLE	WT	ROLE	WT	ROLE	WT
Stability Unstiffened cylindrical shell Nonuniform axial load Compression Bending						

DEPARTMENT OF THE ARMY
U. S. ARMY AIR MOBILITY RESEARCH & DEVELOPMENT LABORATORY
EUSTIS DIRECTORATE
FORT EUSTIS, VIRGINIA 23604

This program was carried out under Contract DA 44-177-AMC-258(T) with Stanford University.

The data contained in this report are the result of research conducted to study the stability of thin-walled unstiffened circular cylindrical shells under nonuniformly distributed axial load. Results are presented for tests on many shells as well as for many tests on a single shell.

The report has been reviewed by this Directorate and is considered to be technically sound. It is published for the exchange of information and the stimulation of future research.

This program was conducted under the technical management of Mr. James P. Waller, Structures Division.

Task 1F162204A17001
Contract DA 44-177-AMC-258(T)
USAAVLABS Technical Report 69-33
November 1971

STABILITY OF THIN-WALLED UNSTIFFENED CIRCULAR CYLINDRICAL SHELLS UNDER NONUNIFORMLY DISTRIBUTED AXIAL LOAD

By

W. H. Horton
J. W. Cox

Prepared by

Stanford University
Stanford, California

for

EUSTIS DIRECTORATE
U. S. ARMY AIR MOBILITY RESEARCH AND DEVELOPMENT LABORATORY
FORT EUSTIS, VIRGINIA

SUMMARY

This report presents an experimental study of the stability of thin-walled unstiffened circular cylindrical shells under nonuniformly distributed axial load. It demonstrates that such shells will buckle when the stress at any point on their surface reaches the critical value for uniform axial compression.

It is furthermore demonstrated that statistical data with regard to shell buckling can be obtained from limited tests on single specimens.

TABLE OF CONTENTS

	Page
SUMMARY	iii
LIST OF ILLUSTRATIONS	vi
LIST OF TABLES	viii
LIST OF SYMBOLS	ix
INTRODUCTION	1
SHELL SPECIMEN FOR FIRST SERIES OF TESTS	10
TEST PROCEDURE FOR FIRST SERIES OF TESTS	12
RESULTS OF THE FIRST SERIES	21
DISCUSSION OF THE RESULTS OF THE FIRST SERIES	38
THE SECOND SERIES OF TESTS	39
Test Specimens	39
Test Procedure	40
DISCUSSION OF THE RESULTS OF THE SECOND SERIES	43
CONCLUSIONS	66
REFERENCES	67
APPENDIX	
Statistical Treatment of the Results of the First Series of Tests	68
DISTRIBUTION	77

LIST OF ILLUSTRATIONS

Figure		Page
1	A Normal Distribution of Buckling Loads	5
2	Fully Developed Buckle Population in a Thin-Walled Cylindrical Shell Under Uniform Axial Compression	6
3	Buckle Pattern 25% Developed	6
4	Buckle Pattern 50% Developed	7
5	Buckle Pattern 75% Developed	7
6	Observation of Buckle Formation With Increasing Load for the Cylinder of Figure 2 With Central Loading	8
7	Cross Section of Test Vehicle Together With Restraining Mandrel	9
8	Stress-Strain Curve for Material of the Series 2 Shell Specimens	11
9	Loading Arrangement for Series 1 Tests	14
10	Unsymmetrical Distributed Loading - Type A	15
11	Two-Place Symmetrical Distributed Loading - Type A	16
12	Three-Place Symmetrical Distributed Loading - Type A	17
13	Two-Place Symmetrical Distributed Loading - Type B	18
14	Three-Place Symmetrical Distributed Loading - Type B	19
15	Typical Buckling Failures, Series 1 Shell Specimens	20
16	Results of Testing a Sample of 40 Cylindrical Shells, Unsymmetrical Distributed Loading - Type A, Loaded Fraction of Perimeter = .50	22
17	Results of Testing a Sample of 25 Cylindrical Shells, Unsymmetrical Distributed Loading - Type A, Loaded Fraction of Perimeter = .86	23
18	Results of Testing a Sample of 50 Cylindrical Shells, Two-Place Symmetrical Loading - Type B, Loaded Fraction of Perimeter = .50	24

Figure		Page
19	Buckling Load as a Function of Fraction of Perimeter Loaded for Series 1 Shell Specimen - Type A Loading	25
20	Buckling Load as a Function of Fraction of Perimeter Loaded for Series 1 Shell Specimen - Type B Loading	26
21	Cross Section of Series 2 Test Vehicle With Restraining Mandrel and Testing Jig	41
22	Series 2 Test Vehicle and Loading Jig in Testing Machine	42
23	Stress-Strain Curve for Material of the Series 1 Test Specimen	45
24	Results of Circular Traverse of Loading for the Shell Specimen of Series 2 Tests, Eccentricity of Load = 3/8r . . .	49
25	Results of Circular Traverse of Loading for the Shell Specimen of Series 2 Tests, Eccentricity of Load = 1/2r . . .	52
26	Maximum Buckling Rate Load for Eccentric Loading at Eight Equally Spaced Circular Positions	55
27	Initial Buckling Region of Shell Specimen of Series 2 Tests as Revealed by Circular Traverses of Loading	56
28	Results of Radial Traverse of Loading for the Shell Specimen of Series 2 Tests	60
29	Cumulative Distribution of Buckles as a Function of Load, Shell Specimen of Series 2	62
30	Buckle Patterns for Six Eccentric Load Positions, Series 2 Shell Specimens	63
31	Total Buckle Population as a Function of Load Eccentricity, Shell Specimen of Series 2 Tests	64
32	Maximum Buckle Rate Load Versus Load Eccentricity, Shell Specimen of Series 2 Tests	65

LIST OF TABLES

Table		Page
I	Unsymmetrical Distributed Loading - Type A	27
II	Two-Place Symmetrical Distributed Loading - Type A	30
III	Three-Place Symmetrical Distributed Loading - Type A . . .	32
IV	Two-Place Symmetrical Distributed Loading - Type B	34
V	Three-Place Symmetrical Distributed Loading - Type B . . .	36
VI	Circular Traverse of Loading for the Shell Specimens of Series 2 Tests	46
VII	Central Axis Loading for the Shell Specimen of Series 2 Tests	57
VIII	Radial Traverse of Loading for the Shell Specimen of Series 2 Tests	58
IX	Treatment of Experimental Data Given in Figure 19	69
X	Treatment of Experimental Data Given in Figure 20	74

LIST OF SYMBOLS

N	population
$\Delta N/N$	fraction of population of buckling loads having values in load intervals $P + \Delta P$
σ	standard deviation
P	applied load
$\bar{P}$	population mean buckling load
R/t	ratio of radius to skin thickness
Δ	distance of load from axis of shell
f_b	axial stress in shell
M	bending moment
Z	modulus of the section
r	shell radius
E	Young's modulus of elasticity
F	f_i, $\bar{f}$, f
t	skin thickness

INTRODUCTION

The behavior of circular cylindrical shells under uniformly distributed axial compression is a subject which has received much attention from theoreticians and experimentalists alike. However, in practice many cylindrical shells are used under conditions in which this idealized load distribution is neither achieved nor even approached. Many cases can be cited in real engineering structures where concentrated loads are diffused into a shell, and many other cases in which other nonuniform systems are encountered can be found readily. An important group, for example, is that in which axial compression is associated with flexure.

In 1932, Flügge[1] investigated the buckling of cylindrical shells under combined bending and compression and derived the interaction relationship for a particular radius-to-thickness ratio and a special longitudinal buckle half wavelength radius ratio. For the case which he considered, he demonstrated that the ratio of the maximum critical stress for bending alone would, within the terms of his analysis, be 33 percent greater than the critical stress for pure compression. Timoshenko,[2] in his theory of elastic stability, referenced this work but omitted the required qualification with regard to buckle wavelength. In 1934, Donnell[3] presented his paper, "A New Theory for the Buckling of Thin Cylinders Under Axial Compression and Bending", to the Fourth International Congress for Applied Mechanics. He noted, as a result of this work, that in pure bending, buckling takes place when the stress at a point in the cylinder wall about 45 degrees to the neutral axis rises to the value which produces failure in uniformly stressed specimens. Despite this conclusion, the validity of Flügge's specific result has been accepted by many until quite recently.

In 1959, Abir and Nardo[4] published their paper on "Thermal Buckling of Circular Cylindrical Shells Under Circumferential Temperature Gradients". They reached the conclusion that the axial buckling stress under variable thermal stress conditions is close to the critical stress of the cylinder when it is subjected to uniform axial compression, if the variation of the intensity of the thermal stress is not large within a half wavelength of the buckling pattern. This work was followed by a study made by Bijlaard and Gallagher[5] on the "Elastic Stability of a Cylindrical Shell Under Arbitrary Circumferential Variation of Axial Stress". The prime conclusion of this research was that the cylindrical shell buckles when the stress at some point reaches the critical stress for a cylindrical shell under uniformly distributed axial compression. Seide and Weingarten,[6] in 1961, reported their work, "The Buckling of Circular Cylindrical Shells Under Pure Bending." Their analysis showed that the maximum critical bending stress would, for all practical purposes, equal the critical compressive stress.

Experimental work to support these theoretical considerations has been remarkably lacking. It is true that in 1933 Lundquist[7] published a note on "Stress Tests of Thin-Walled Duraluminum Cylinders in Pure Bending", while in more recent times Suer, Harris, Skene, and Benjamin[8] published a partially experimental, partially theoretical paper which treated the bending stability of thin-walled unstiffened circular cylinders, including the effects of internal pressure. The most recent contribution is an experimental study made by Heise.[9] This work, which was published after the present investi-

gation was well in hand, bears direct comparison with part of the work reported herein. Heise uses a very similar circular traverse system in the determination of the quality of his test vehicles. The main difference lies in the definition of the buckling load. However, there still appears to be a great need for experimental studies to provide practical confirmation of existing theoretical opinions.

In view of the practical application of such information, a program of experimental studies was undertaken in this field. Investigations were made not only of those cases in which there is a smooth variation in load distribution but also of those in which there are sharp discontinuities in the loading actions. Studies were made of load distributions in which flexure as well as compression was present.

Recent researches on the behavior of cylindrical shells under uniform axial compression have shown in a positive fashion that the experimental approaches of the past have been far too restrictive in outlook. New and powerful techniques have been and are being developed to improve this situation. A new philosophy with regard to experimental studies on the buckling of shell bodies has recently been presented by Horton.[10] The work which he reports has shown that there are two basic statistical approaches which can be taken in such studies: the first is to consider a population of nominally identical specimens, and the second is to consider a population of buckles within the test vehicle itself.

In the work reported here, both approaches have been made. They lead to the same conclusion; namely, that irrespective of the nature of the distribution of load around the periphery of the shell, buckling takes place when the stress reaches the level which would be critical for uniform load conditions.

With regard to the classic approach (namely, that of a population of nominally identical specimens), it was reasoned that if the tests were performed using shell specimens of consistently high quality, both in uniformity of geometry and in material properties, then the initial imperfections would most likely be randomly distributed and the buckling load resulting from the test of a single specimen could be regarded as one member of a population of buckling loads for that test configuration. It was further reasoned that statistical properties of the population, such as mean value and distribution of values about the mean, could be estimated from a random sample of buckling loads obtained from identical tests of several specimens. The effect on shell buckling strength of two different distributions of loading would then be detected from a comparison of the statistical properties of their respective populations of buckling loads.

It is reasonable to expect that for shell specimens such as described above, the buckling loads for a given test configuration would be distributed normally; i.e., according to the normal law of error. In his treatment of the subject of scientific research, Wilson[11] points out that it appears to be safe to use the normal law for observations where four or more sources of error enter with about equal weight. This would be the expected case

for the reported buckling tests. For cylinders manufactured to high and carefully controlled quality standards, errors introduced by initial imperfections in the shell body are expected to be of equal weight with those errors introduced through the testing machine, through the loading heads, and through repeated adjustment of the overall setup between the tests in a given sequence.

The mathematical statement of the normal law is well-known and for application in the present instance will be written as

$$\frac{\Delta N}{N} = \frac{1}{\sigma\sqrt{2\pi}} e^{\frac{-(P-\bar{P})^2}{2\sigma^2}} \Delta P \qquad (1)$$

where $\Delta N/N$ is the fraction of population of observed buckling loads having values in the load interval $P + \Delta P$, and where $\bar{P}$ and σ are the population mean buckling load and standard deviation, respectively. Figure 1 shows graphically the statistical properties of a population of buckling loads distributed in a normal manner. Thus, for such a population it appears that a comparison of the $\bar{P}$ and σ values provides a sufficient basis for showing the effect of load distribution on the buckling strength of a cylindrical shell structure.

The problem, of course, from an experimental point of view is the manufacture and acquisition of a large number of test vehicles. This is a question of such importance that it merited careful investigation. A novel solution was found in the can manufacturing industry.

The manufacture of cans is a fully automated process. It has been developed to the extent that such devices are readily and economically obtainable. They are vehicles which, to a large degree, can be considered of a similar character. There is, in fact, an almost infinite population available, if required.

There is, as we mentioned before, another approach to this problem: the approach which considers a population of buckles within the test vehicle itself. It is to this approach that we now direct our attention. Buckle population studies can be made only if it is possible to generate a population of sufficient size and character to be studied statistically. The photograph given in Figure 2 shows a fully developed buckle population in a thin-walled cylindrical shell under uniform axial compression. As you will see, this is a complete buckling of the shell. The buckles are all identical in character. In Figures 3 through 5, various stages of a test are carried out with this process; the resulting load population curve shown in Figure 6 is recognized to be the normal logistic curve. It is essential in the operation of this kind of test procedure that precautions are taken to ensure that the buckle process remains elastic throughout the test. This leads to the requirement that the depth to which a buckle is permitted to develop be restricted. Restriction is accomplished by means of an inner mandrel. A cross section of the test vehicle, together with this restraining mandrel, is given in Figure 7.

The developments referred to in the previous paragraph are developments which apply only to the case of pure axial compression. However, in this work we are concerned with nonuniform distributions of axial load, and the question which faces us is, Can this technique be modified to deal with this problem? When we consider the complexity of obtaining nonuniform distributions by means of a series of individual loads, or by loading only a small portion of the perimeter, we find that if we wish to attempt to run a large number of tests on a single specimen, the design of the necessary test gear is expensive. However, we recognize that nonuniform distributions of load can be readily and simply obtained by using a combination of compression and flexure. This makes an extremely simple rig and makes it possible to study the effect of quality on buckle characteristics together with the effect of nonuniform distributions of load on the overall buckle behavior. Provided a specimen can be designed in such a manner that its properties are not influenced by repeated tests, we should be able to acquire a large amount of statistical evidence from a single specimen. The method of accomplishing this and the details of the results obtained are given in the main body of the report.

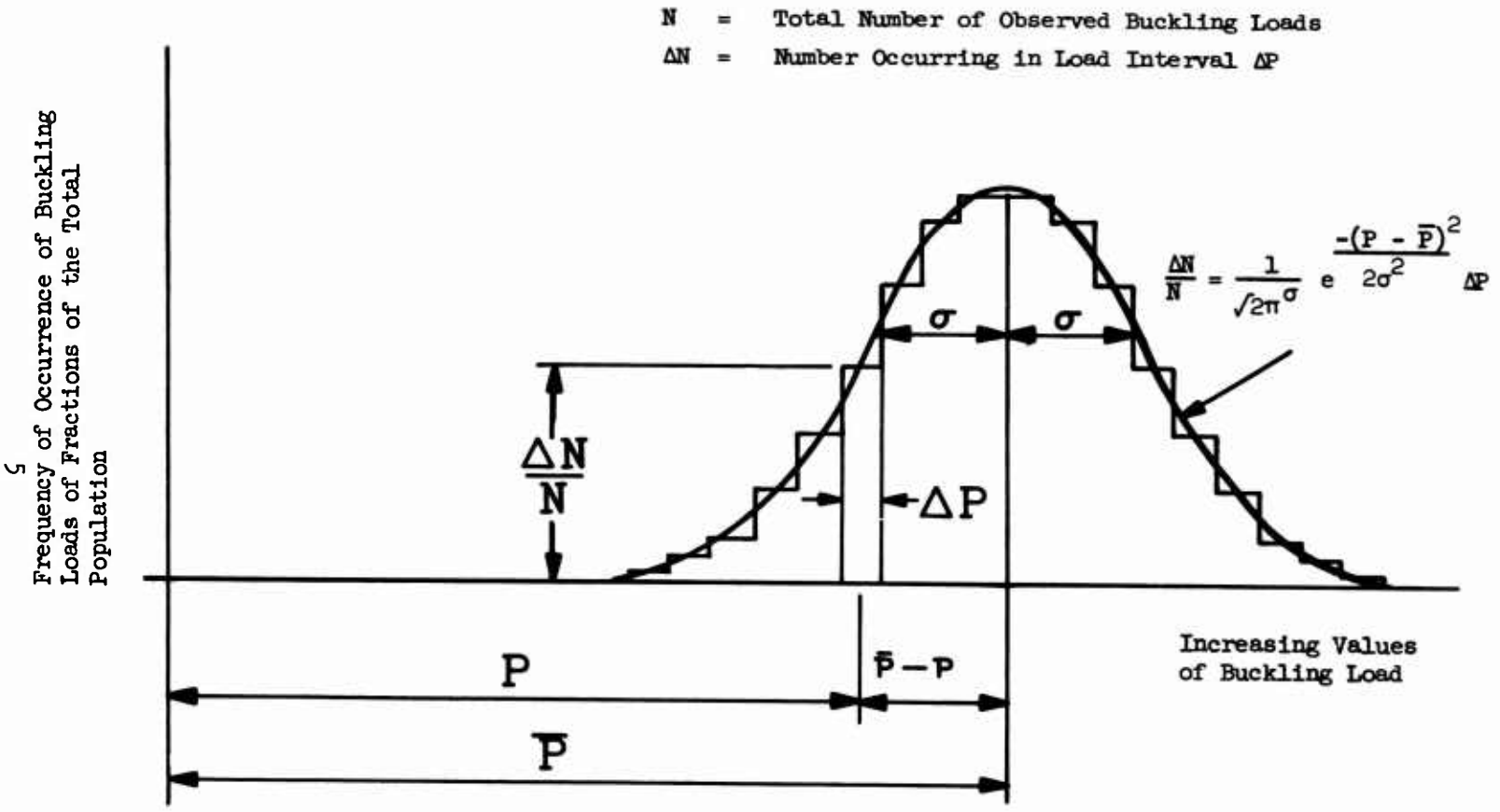

Figure 1. A Normal Distribution of Buckling Loads.

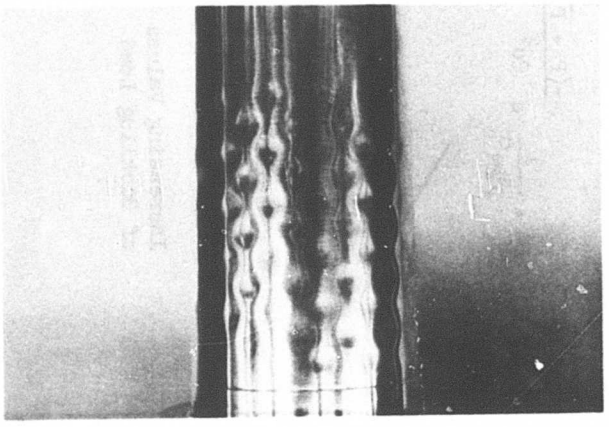

Figure 2. Fully Developed Buckle Population in a Thin-Walled Cylindrical Shell Under Uniform Axial Compression.

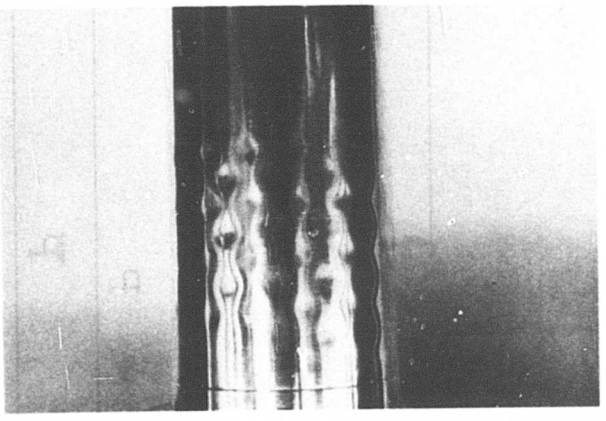

Figure 3. Buckle Pattern 25% Developed.

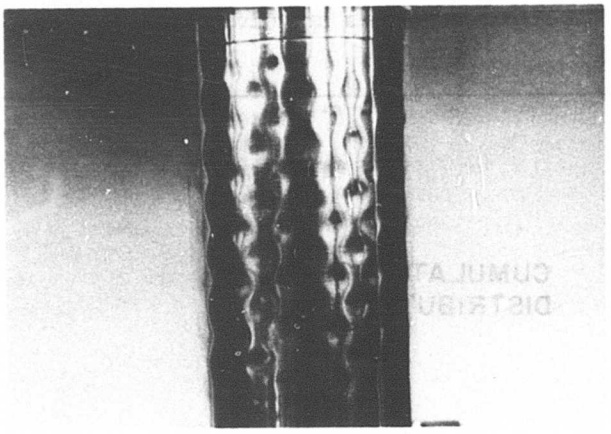

Figure 4. Buckle Pattern 50% Developed

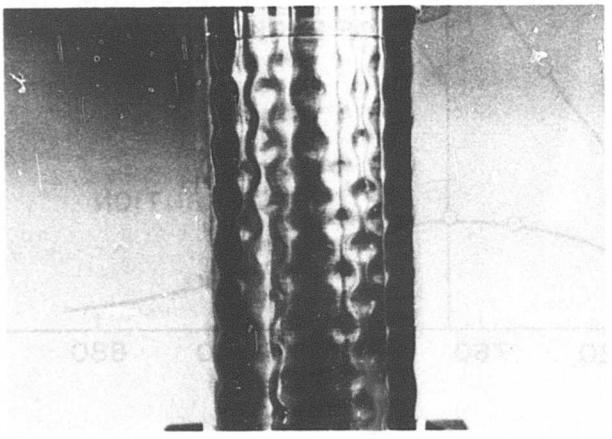

Figure 5. Buckle Pattern 75% Developed.

Experimental Values are Given in Table VII.

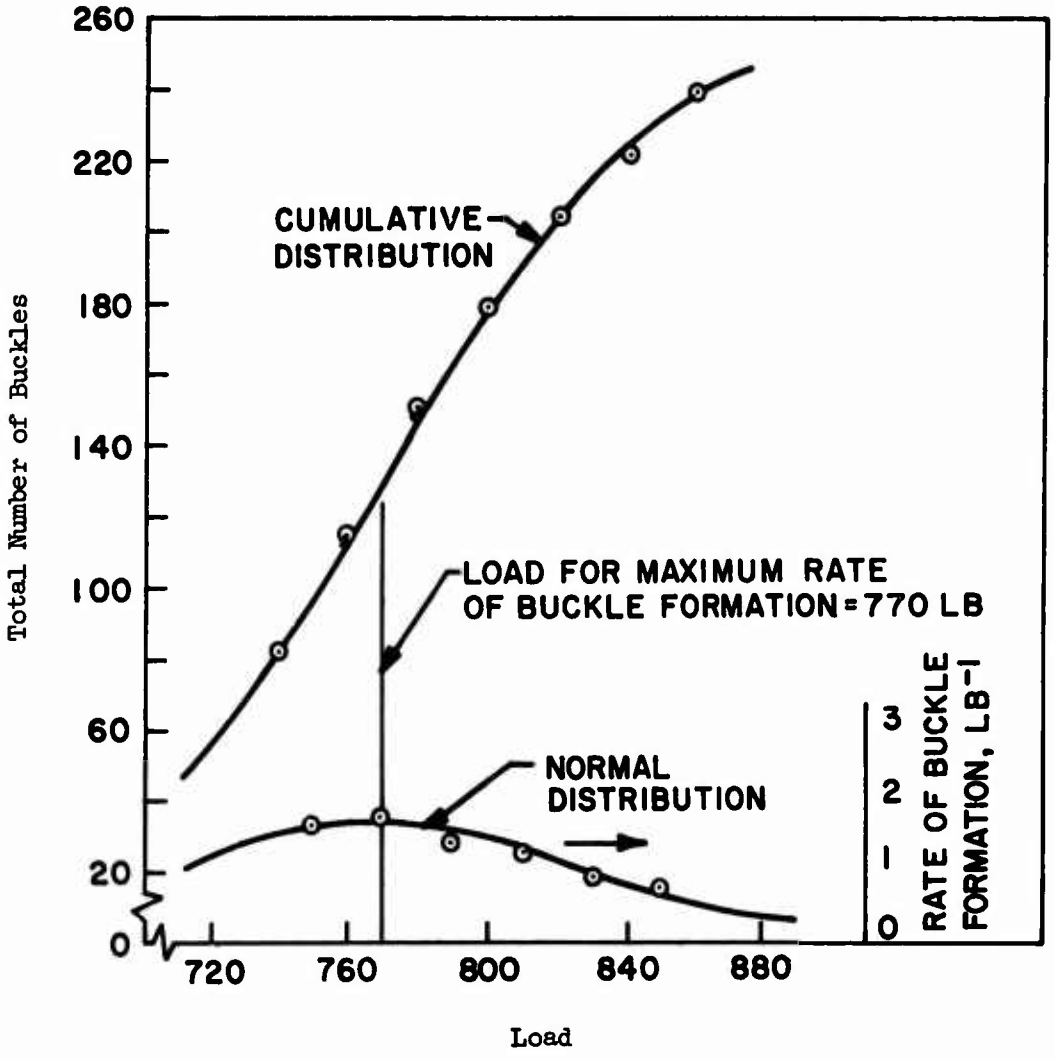

Figure 6. Observation of Buckle Formation With Increasing Load for the Cylinder of Figure 2 With Central Loading.

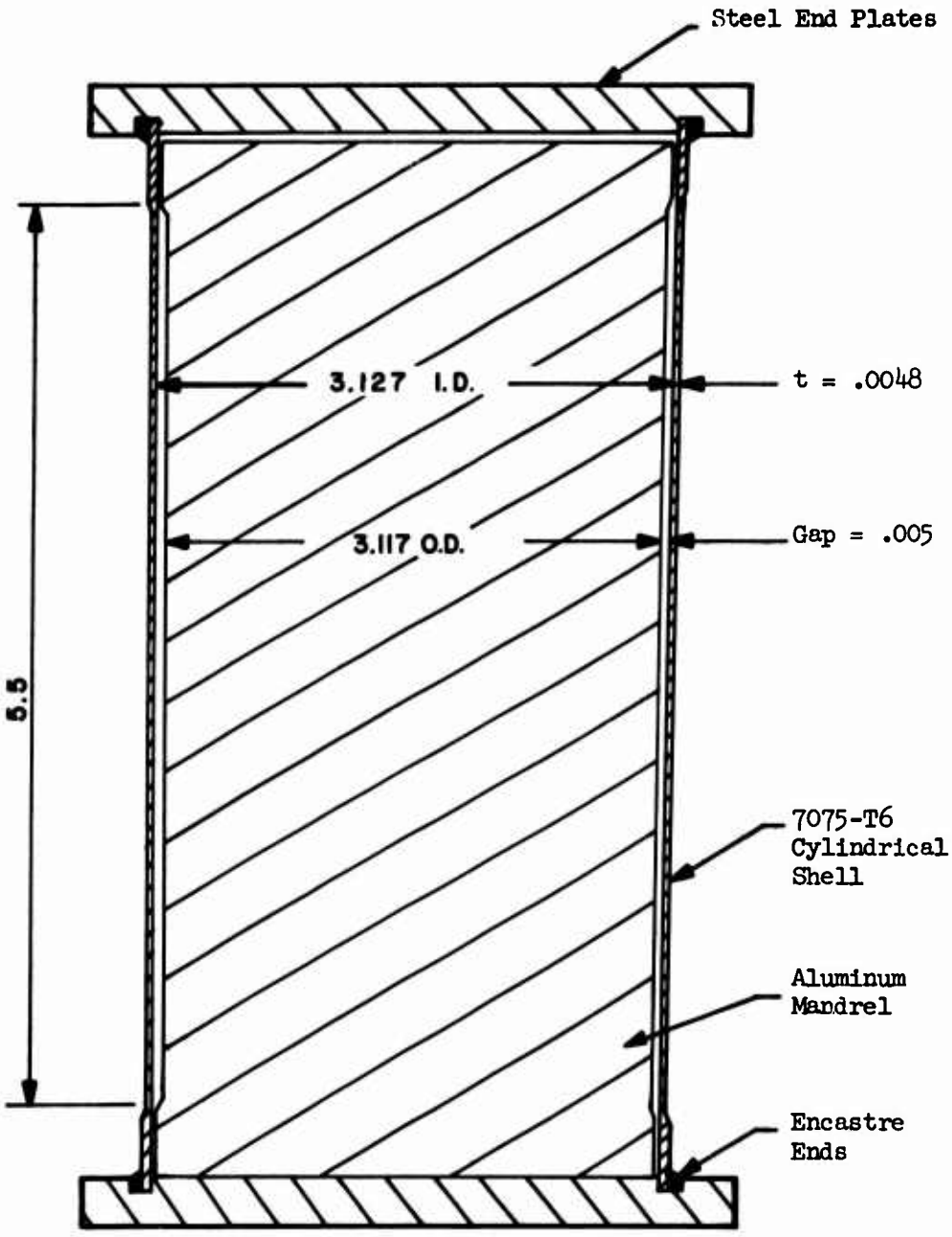

Figure 7. Cross Section of Test Vehicle Together With Restraining Mandrel.

SHELL SPECIMEN FOR FIRST SERIES OF TESTS

In the first series, 349 cylindrical shell specimens were tested. These were all manufactured by mass-production machinery so that variations in geometry from specimen to specimen would be confined within the close tolerance limits essential for successful operation of such equipment.

Blanks for the cylindrical bodies were punched from twice cold-rolled steel sheet supplied from the mill in the form of rolled strips. In one continuous operation these blanks were formed into a cylindrical shape, the edges were prepared and joined by soldering, and a sizing operation on the completed cylinder was performed. Edge restraint was provided through a subsequent operation in which the ends of the cylinders were joined with a steel sheet metal cover by the same process as is used for beverage cans. The shell specimens were then ready for testing.

Completed cylinders were 2.63 inches in diameter and 4.75 inches in length. Shell thickness was .0058 inch, giving an R/t ratio of 226. A typical stress-strain curve for the steel shell material is given in Figure 8.

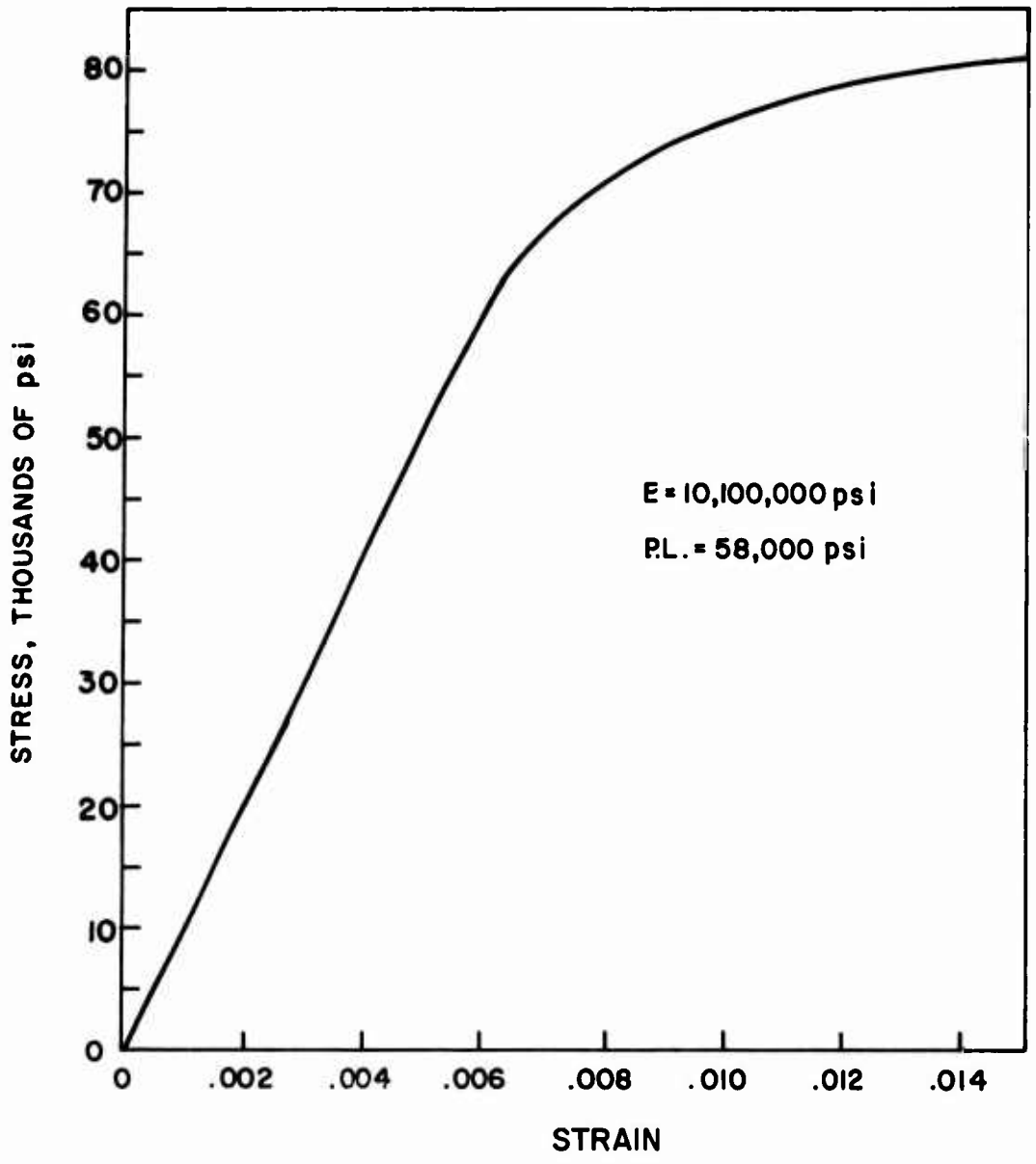

Figure 8. Stress-Strain Curve for Material of the Series 2 Shell Specimens.

TEST PROCEDURE FOR FIRST SERIES OF TESTS

The general arrangement for testing is shown in Figure 9. Loading was applied by either a standard Baldwin-Lima-Hamilton or a Tinius-Olsen testing machine, both of which are of 60,000-lb capacity. The machine load was applied through a spherical loading block in order to minimize the effect of slight variations in parallelism of the specimen ends.

As mentioned previously, three general cases of loading were used. These are shown schematically in Figures 10 through 14. For each case a special set of loading plates was used to distribute the test load around the shell perimeter. These plates were made of 1/4-inch-thick structural grade aluminum and during a test they contacted the specimen along the rings formed by the fabrication joint between the cylinder and the end covers. For example, the set of loading plates for the case of three-place symmetrical loading (Figures 12 and 14) consisted of five pairs of plates, each with three lobes centered 120 degrees apart. One pair each was provided for distributing the load along 18-, 40-, 60-, 80-, and 100-degree segments of the end perimeters. Loading was applied symmetrically with respect to the midplane normal to the shell axis. The manner of arranging a set of plates to give a desired distribution of load is clear from Figure 9.

The end rims mentioned above possessed a degree of flexural stiffness and could resist bending out of the end plane. Advantage was taken of this fact to create two variations on each of the cases of symmetrically distributed loading. These are depicted in Figures 11 and 13 and Figures 12 and 14 for the cases of two-place and three-place symmetrical loading, respectively. The distribution labeled Type B occurs when the end rims are continuous; that is, when the flexural stiffness of the rim participates in the transfer of load from loading plate to shell. By the simple expedient of cutting through the rim at the ends of a loaded segment, the distribution of Figure 10, labeled Type A, was caused to occur. This cutting was done with a thin, high-speed, abrasive wheel without affecting the shell body.

That the Type A and Type B variations of load distribution did occur was shown with the aid of SR-4 electrical resistance strain gages. A number of these having 1/8-inch grid length were placed around an end of a shell specimen so that peripheral distribution of longitudinal strain could be measured. Different load plates were used to distribute loading through both a continuous and a cut rim. Strain measurements from these tests provided the data from which the load distributions shown in Figures 10 through 14 were constructed.

After a specimen had been set up for tests, the machine load was gradually increased. Typically, the load would be observed to rise smoothly until failure by buckling occurred, after which it would suddenly fall off and stabilize at a lower value. If the machine loading process was continued, the load would rise slowly until it was slightly above this initial stable falloff value, and then a second buckling and load falloff sequence would occur. As testing progressed, the initial falloff came to be considered a significant characteristic of the buckling failure, data on which might be of value in planned future experiments.

The data recorded for each test included the buckling load, the location of the failure, the sound of the buckle formation (whether a sharp or a soft snap), and, in most instances, the falloff load. Tables I through V contain all recorded test data from the shell specimens used in the experimental program. Reference is made in each table to the corresponding load distribution diagram of Figures 11 through 14. Typical buckling failures are shown in Figure 15.

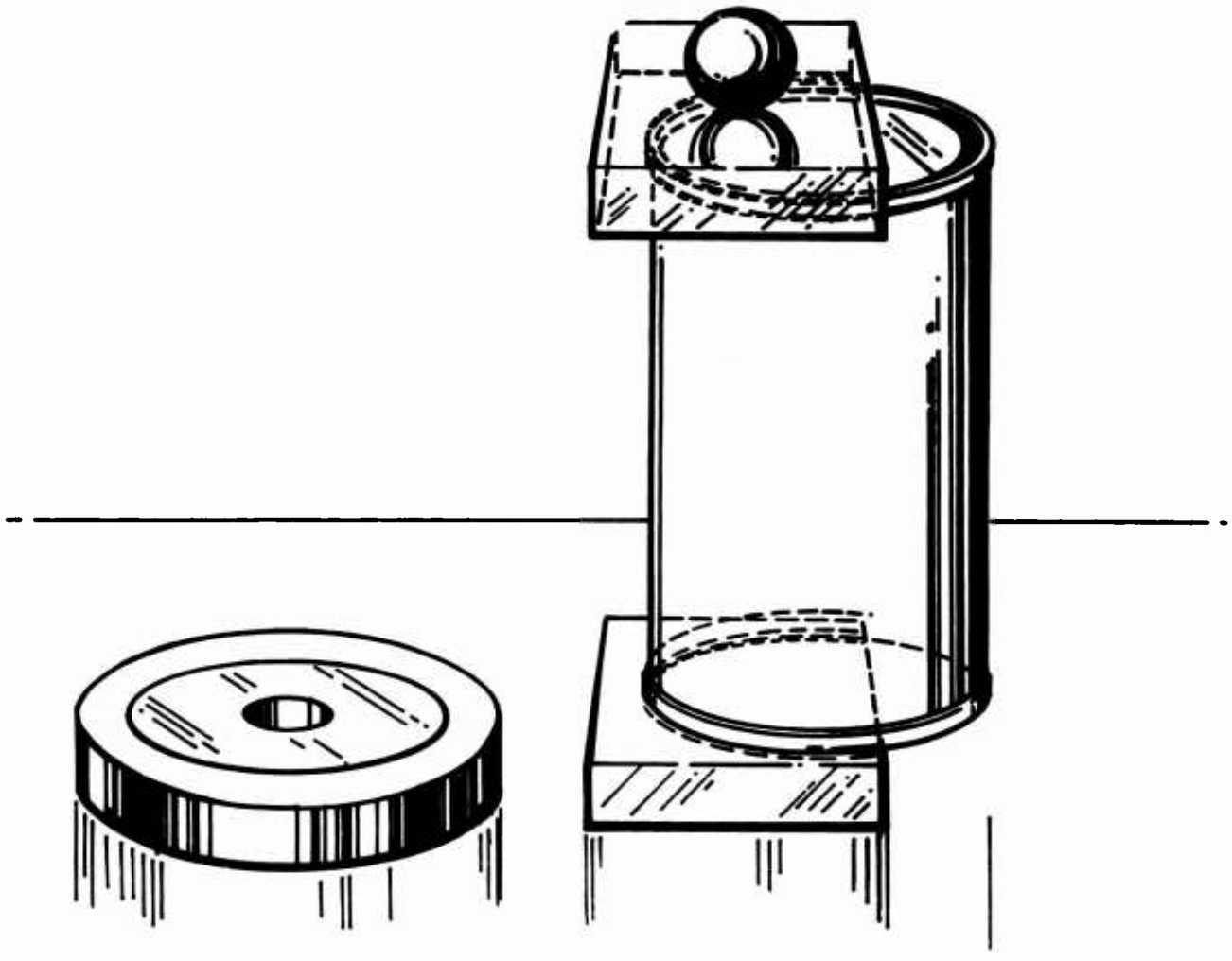

Figure 9. Loading Arrangement for Series 1 Tests.

See Table I

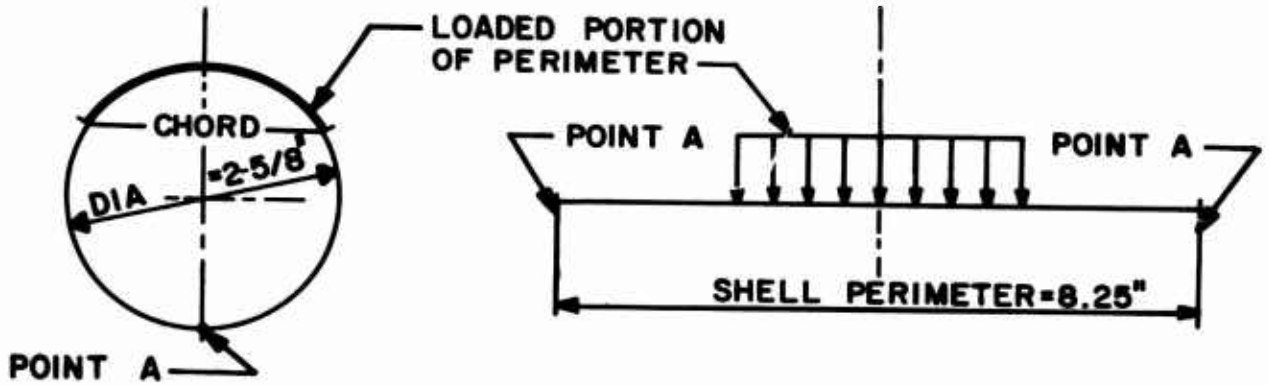

Figure 10. Unsymmetrical Distributed Loading - Type A.

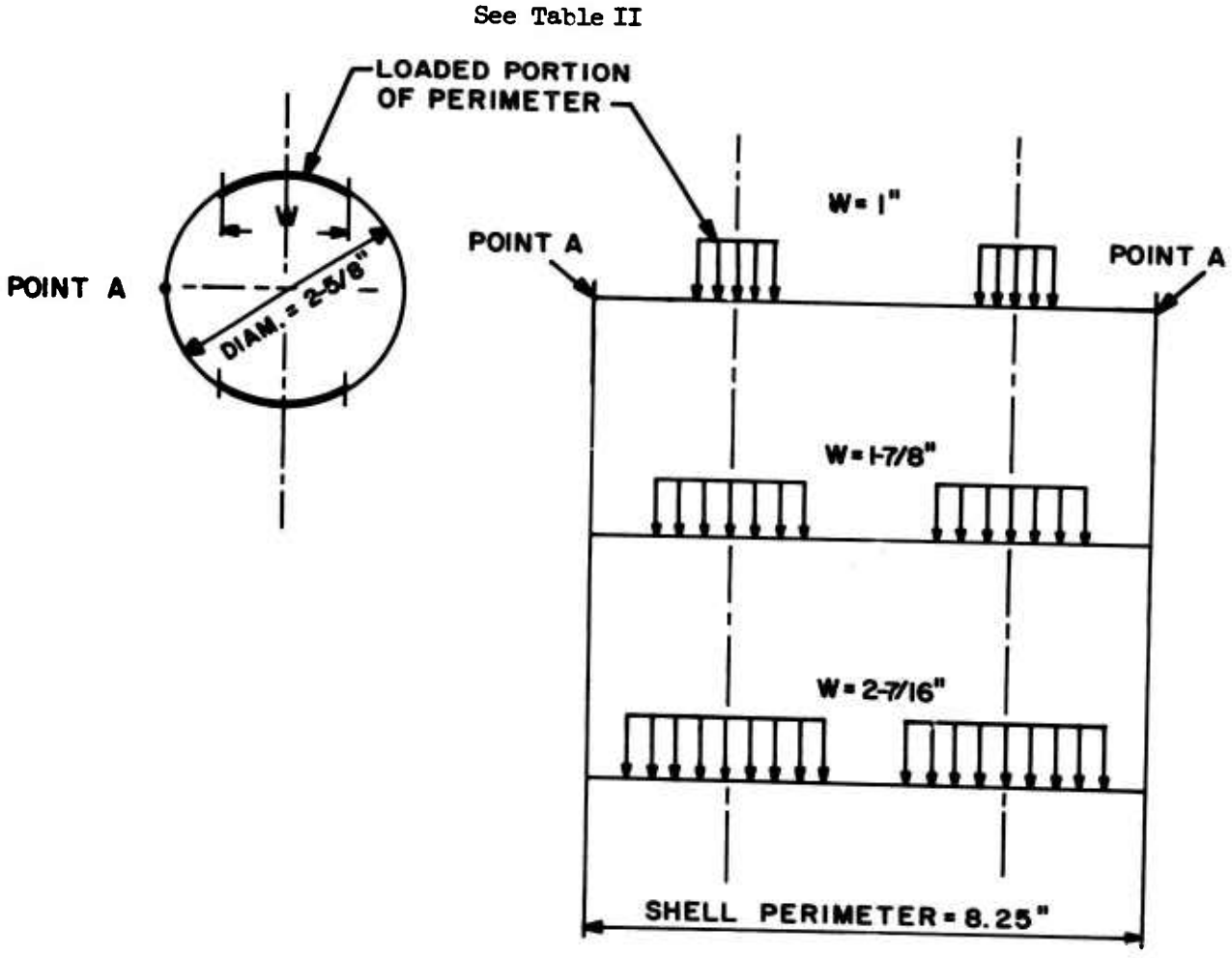

Figure 11. Two-Place Symmetrical Distributed Loading - Type A.

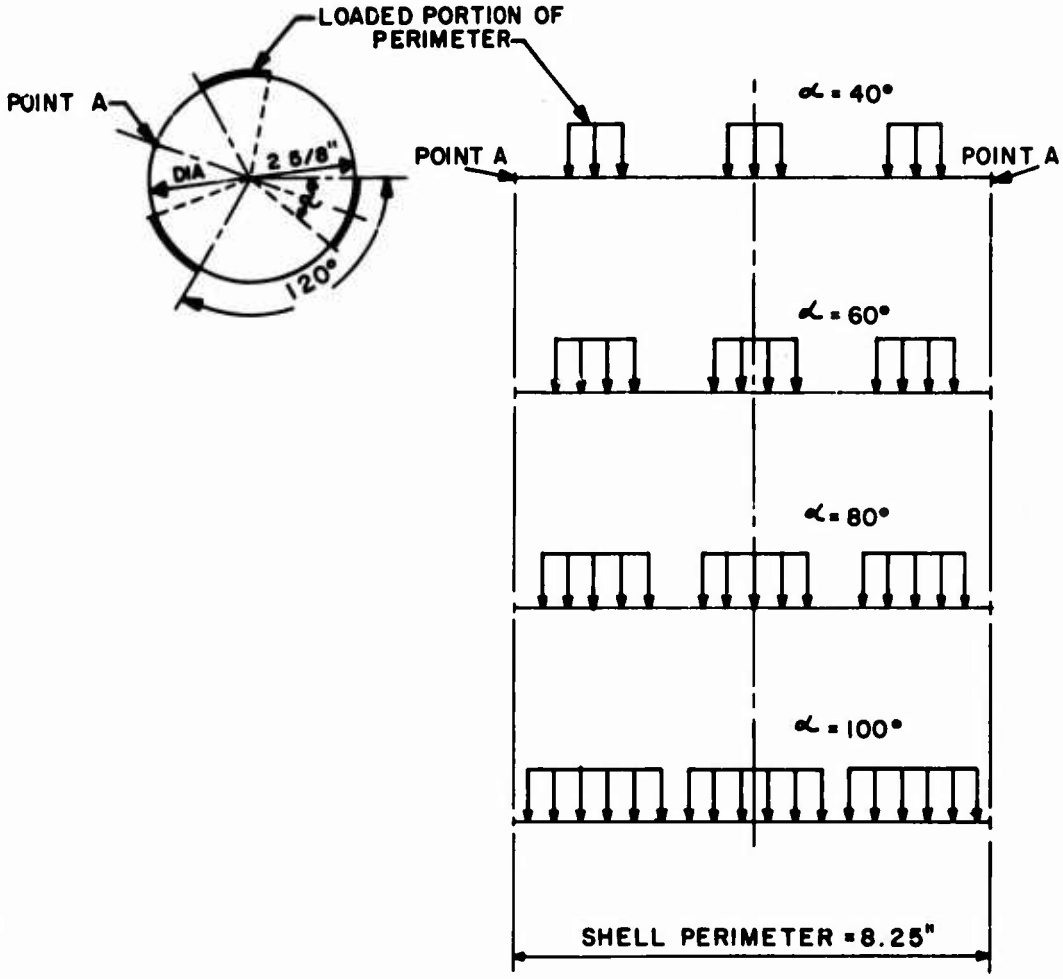

Figure 12. Three-Place Symmetrical Distributed Loading - Type A.

See Table IV

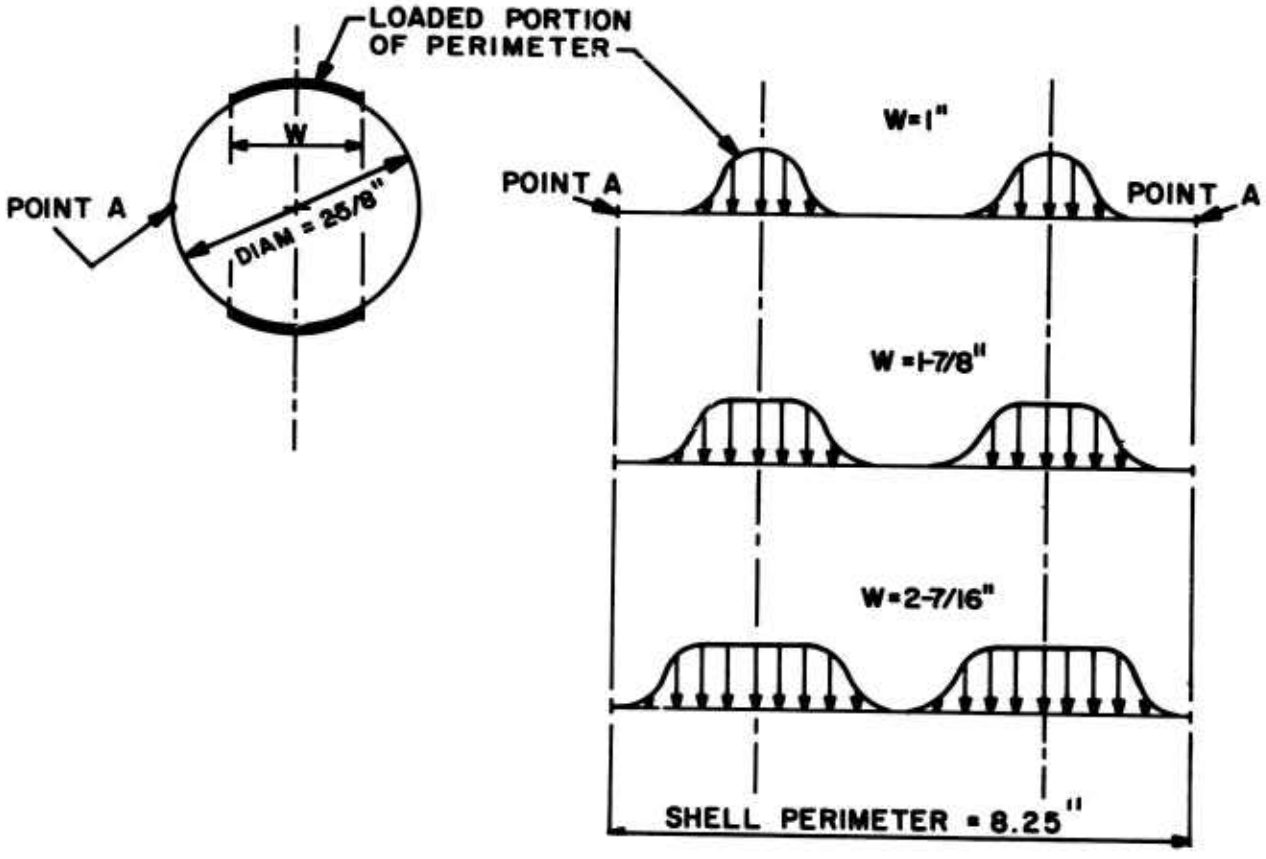

Figure 13. Two-Place Symmetrical Distributed Loading - Type B.

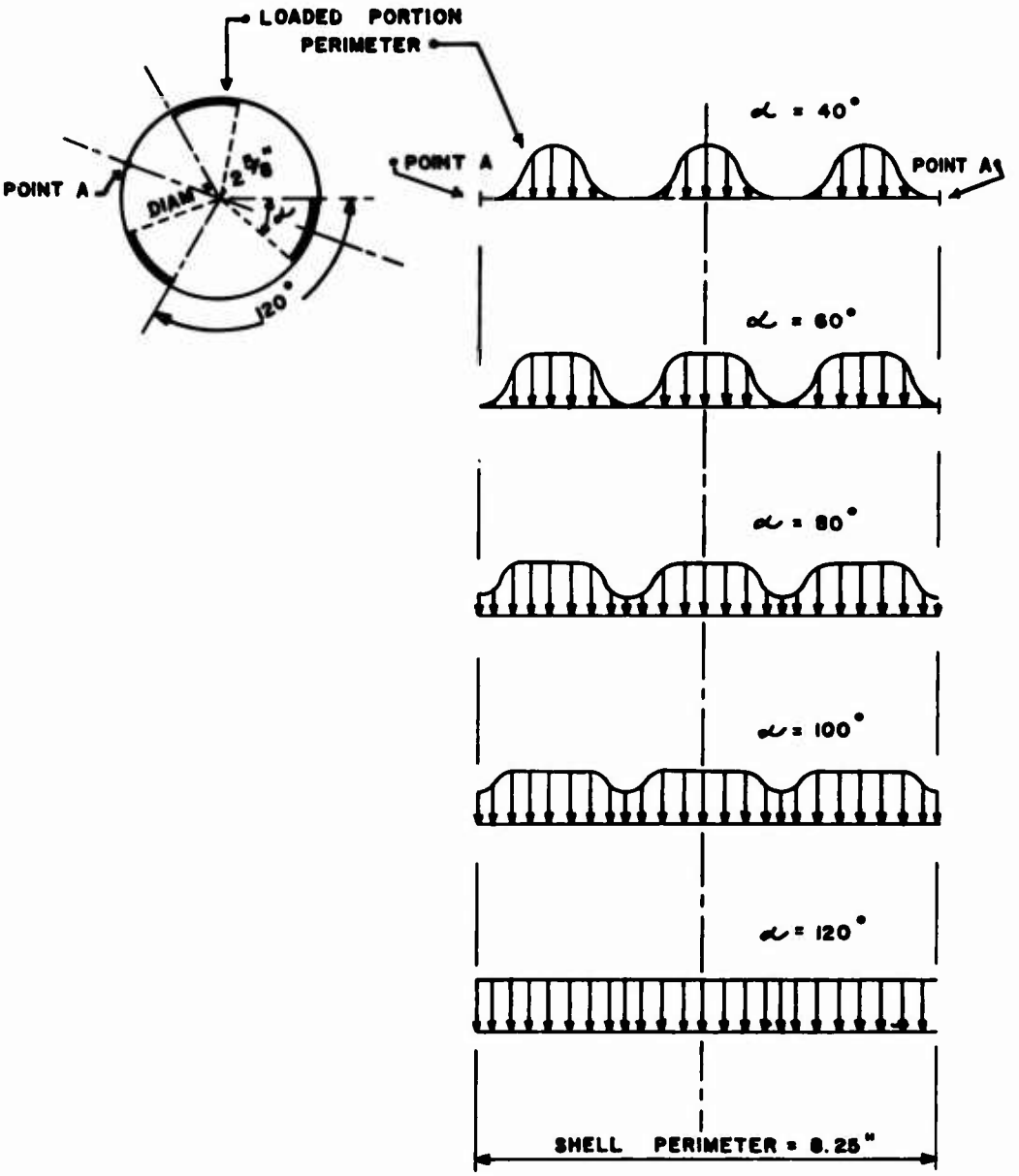

Figure 14. Three-Place Symmetrical Distributed Loading - Type B.

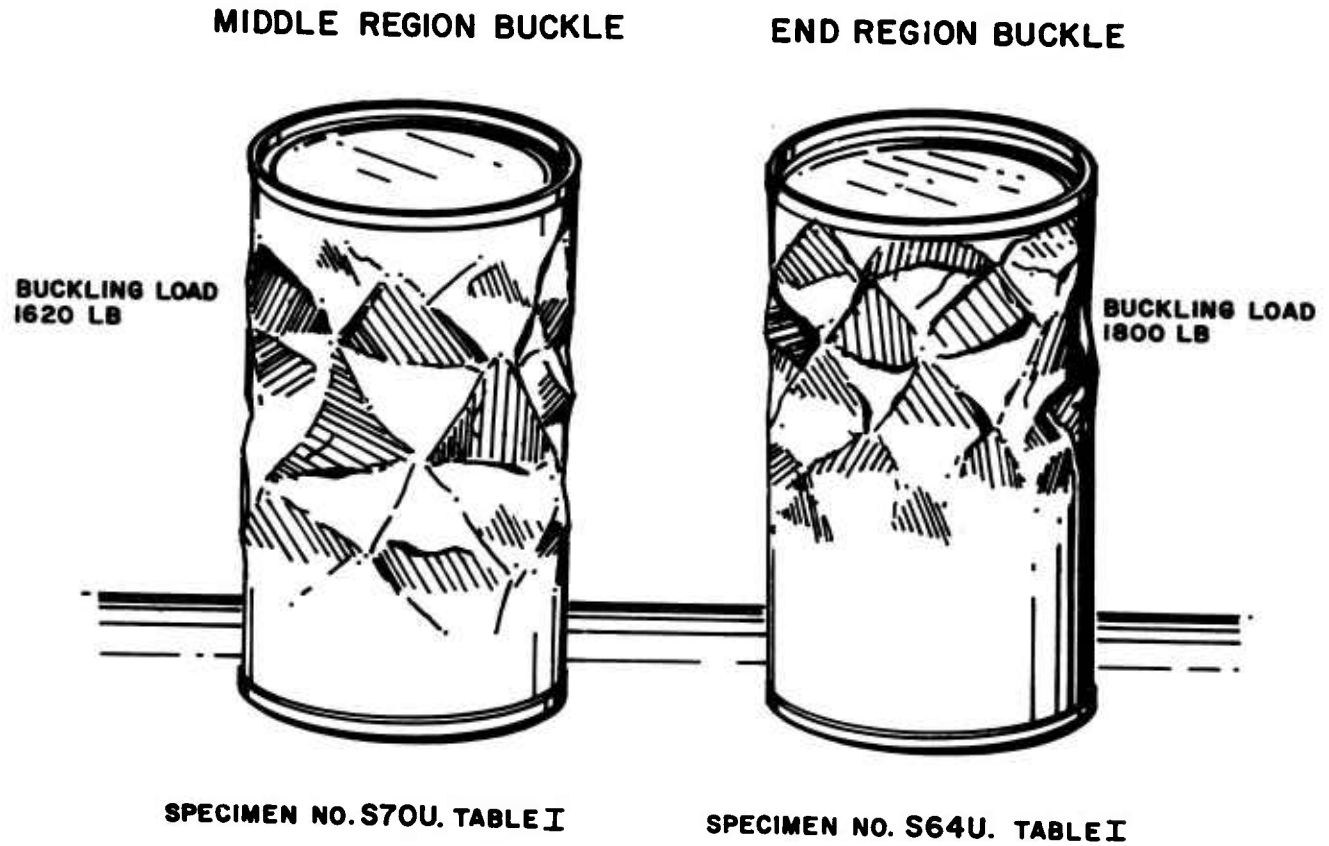

Figure 15. Typical Buckling Failures, Series 1 Shell Specimens.

RESULTS OF THE FIRST SERIES

The critical forces for unsymmetrical loading of the type designated A in the test are presented in Table I. The values for two-place symmetrical loading under the same condition of edge fixity are listed in Table II, while the corresponding levels for three-place loading are given in Table III. Probability plots and cumulative distribution curves for two representative samples of the data outlined above are shown in Figures 16 and 17.

The data relative to two-place symmetrical and three-place symmetrical loading with edge fixity Type B are shown in Tables IV and V, respectively. A probability plot and cumulative distribution curve for an appropriate sample of this information is exhibited in Figure 18. The mean values of compressive load to produce instability are plotted against the percentage of perimeter loaded for types A and B edge conditions in Figures 19 and 20.

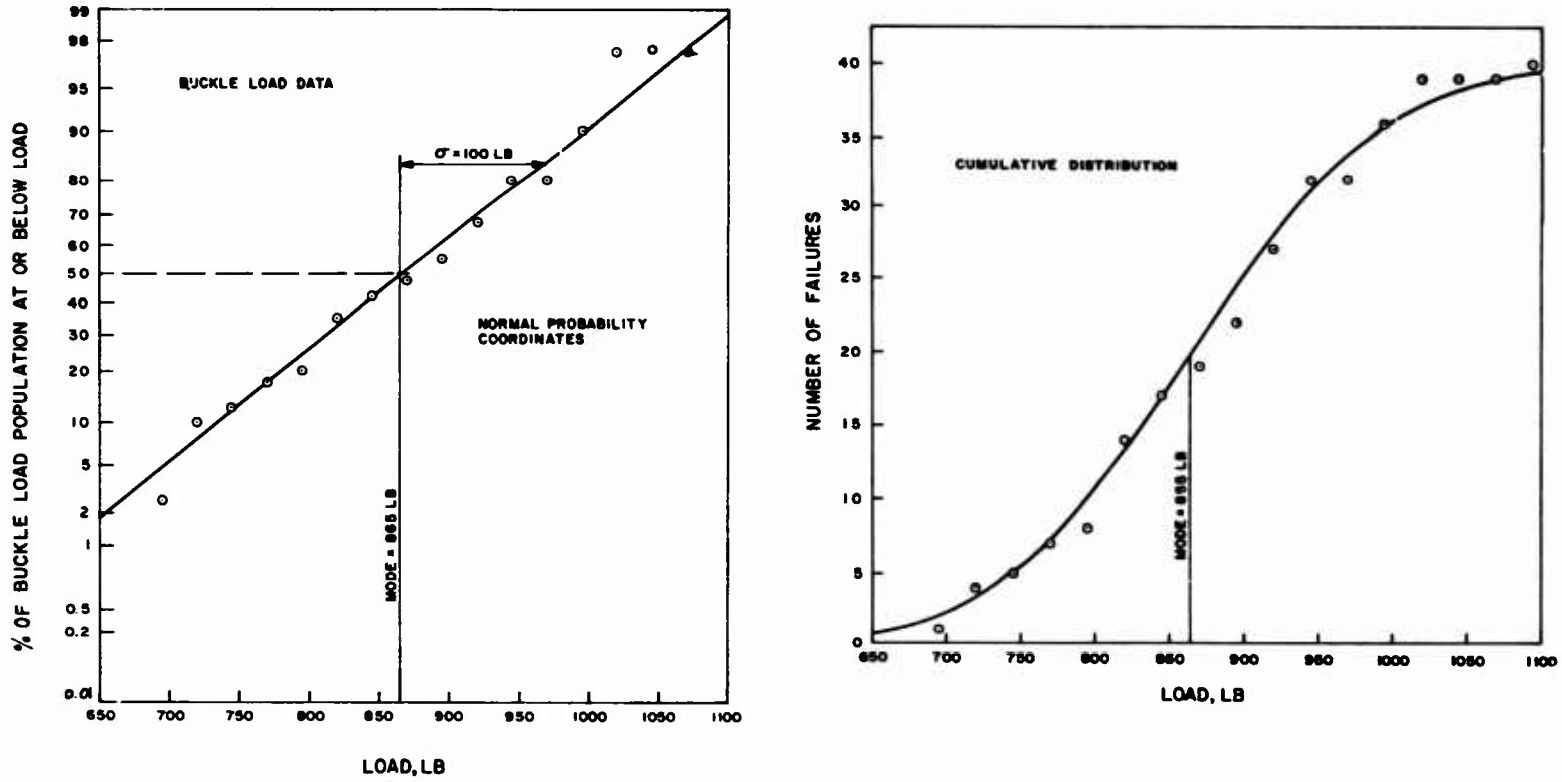

Figure 16. Results of Testing a Sample of 40 Cylindrical Shells, Unsymmetrical Distributed Loading - Type A, Loaded Fraction of Perimeter = .50.

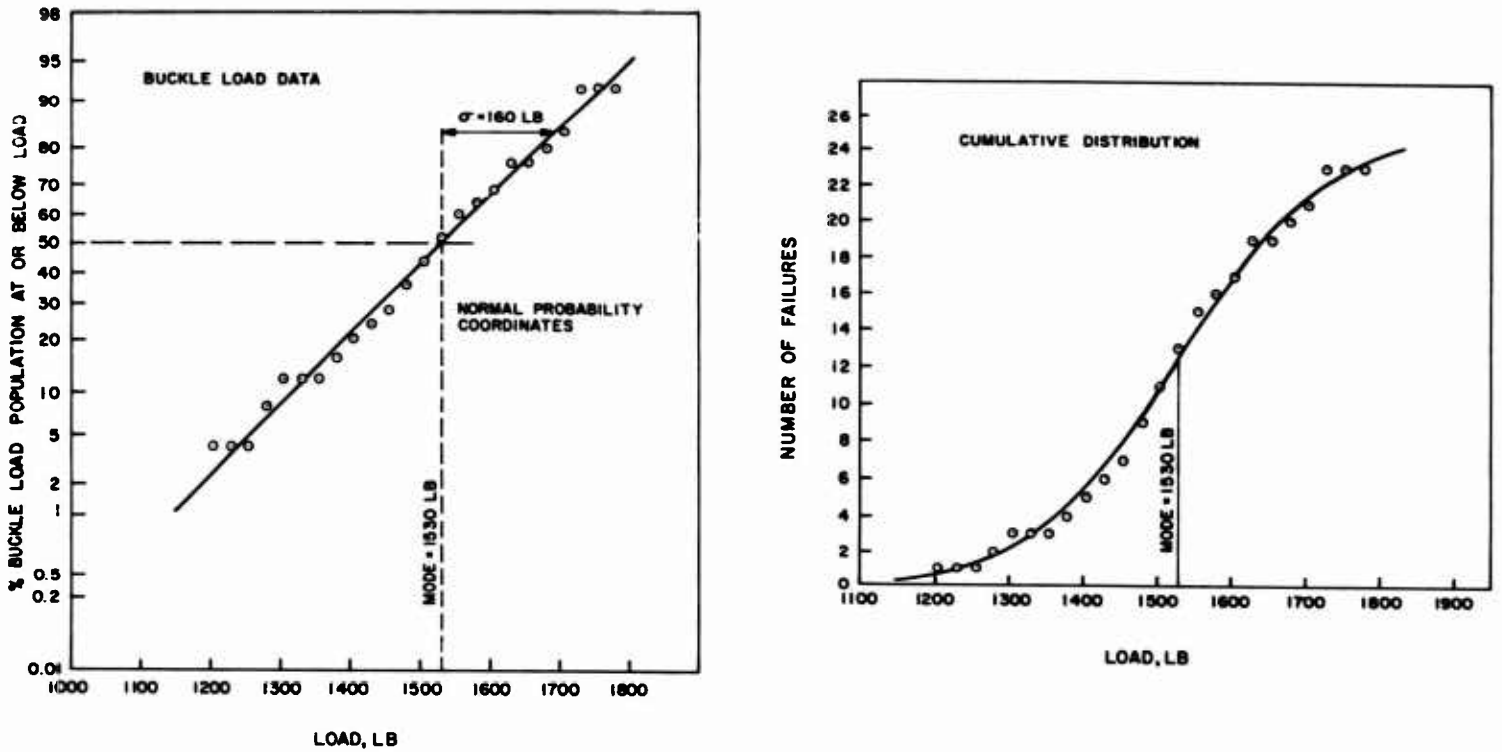

Figure 17. Results of Testing a Sample of 25 Cylindrical Shells, Unsymmetrical Distributed Loading - Type A, Loaded Fraction of Perimeter = .86.

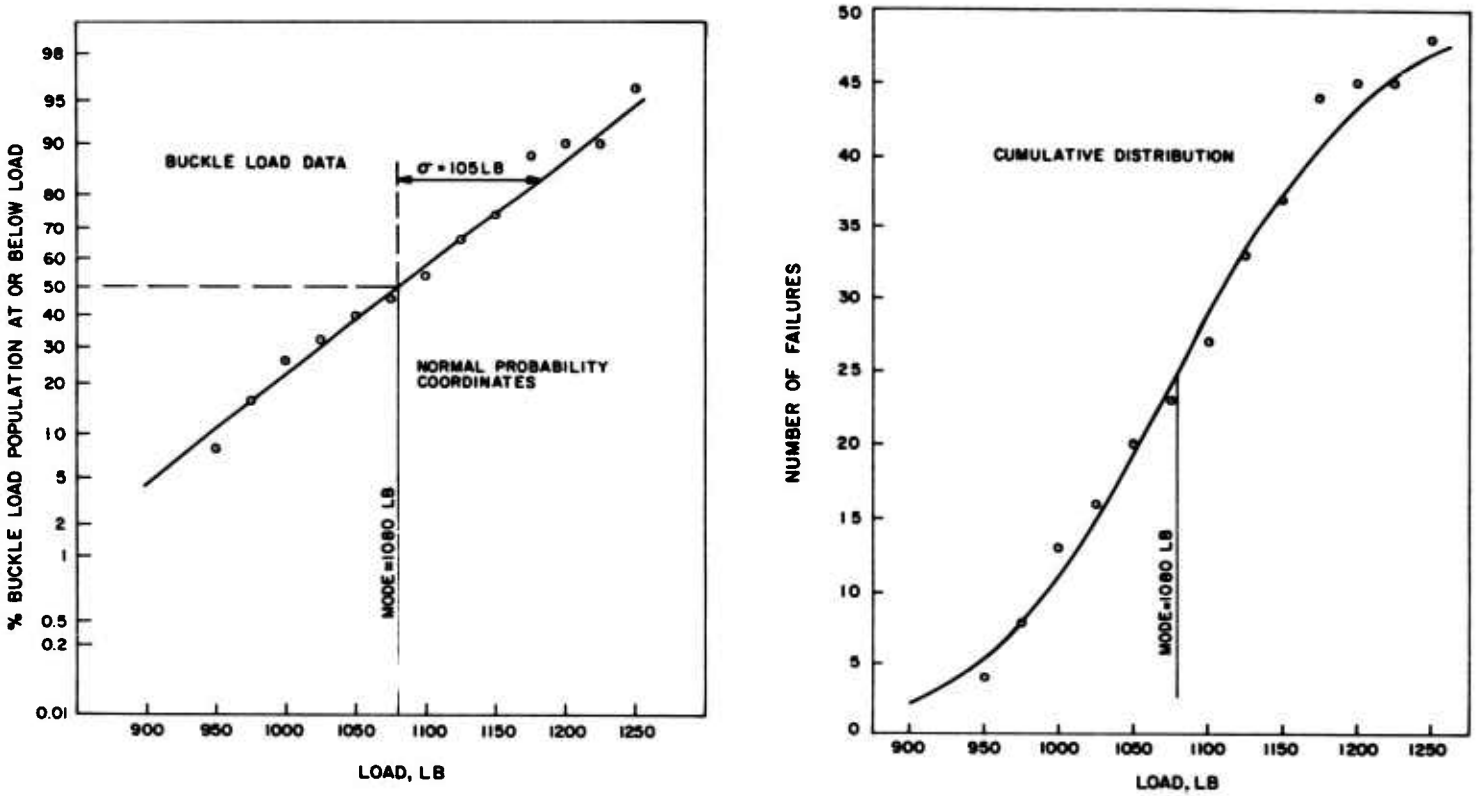

Figure 18. Results of Testing a Sample of 50 Cylindrical Shells, Two-Place Symmetrical Loading - Type B, Loaded Fraction of Perimeter = .50.

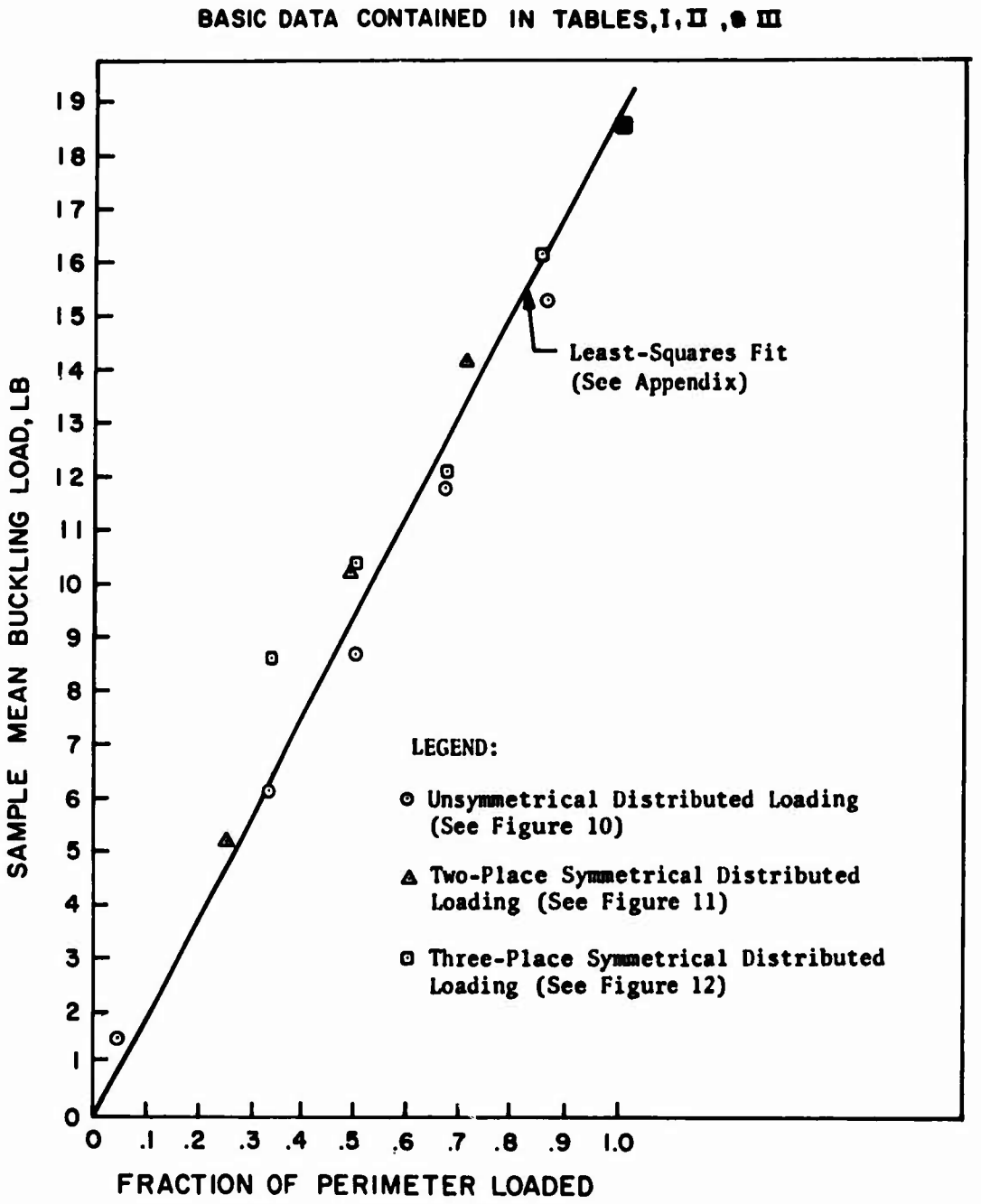

Figure 19. Buckling Load as a Function of Fraction of Perimeter Loaded for Series 1 Shell Specimen - Type A Loading.

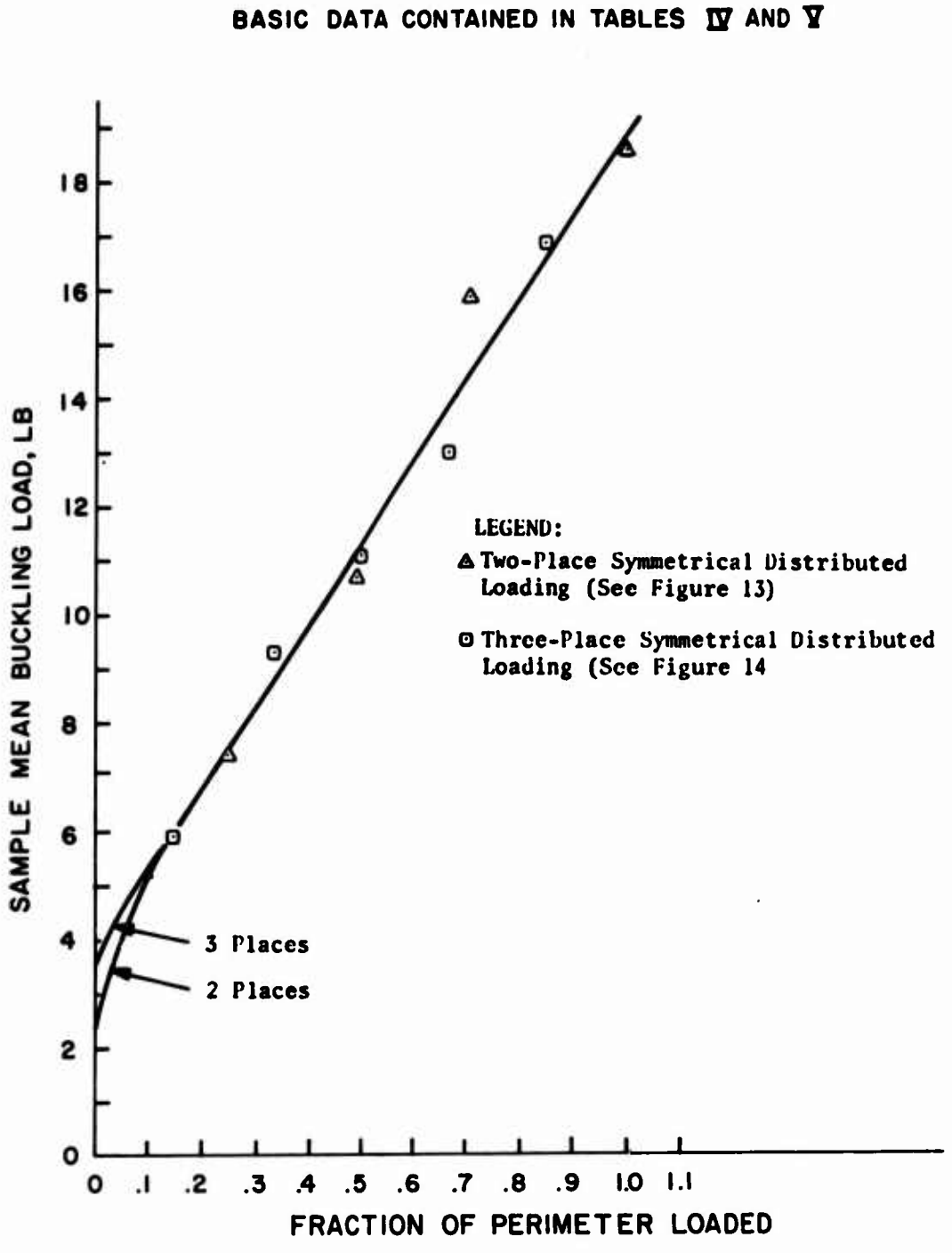

Figure 20. Buckling Load as a Function of Fraction of Perimeter Loaded for Series 1 Shell Specimen - Type B Loading.

TABLE I. UNSYMMETRICAL DISTRIBUTED LOADING - TYPE A
Testing Machine: 60,000-lb Tinius-Olsen
(See Figure 10)

Shell No.	Chord (in)	Perimeter (pct)	Buckle Load(lb)	Buckle Data Location	Snap	Soft	Falloff Load
			GROUP 1 (10 Tests)				
S41U	2-1/4	.33	630	Top	x		440
S42U			510	Bottom	x		340
S43U			590	Top/Middle	x		-
S44U*			620	Upper 1/3	x		460
S45U			740	Top	x		340
S46U			580	Top	x		300
S47U			750	Top	x		380
S48U			600	Top/Middle	xx		480/320
S49U			540	Top	x		420
S50U			640	Top	x		320
			GROUP 2 (40)				
S1U	2-5/8	.50	840	Top	xx		720/580
S2U			990	Top/Middle	xx		820/640
S3U*			900	Bottom/Middle	xx		840/680
S4U			930	Top	x		640
S5U			900	Top		x	700
S6U			850	Middle	xx		770/520
S7U			840	Top/Middle	xx		780/520
S8U			810	Top/Middle	x		560
S9U			820	Top		x	-
S10U*			740	Top	x		500
S11U*			1080	Middle	xx		600/460
S12U			1000	Top	xx		820/500
S13U			760	Top	x		460
S14U			890	Top	x		520
S15U			1000	Top	x		520
S16U			810	Top	x		480
S17U			690	Top		x	620
S18U			840	Bottom	xx		680/480
S19U			700	Top	x		470
S20U			790	Top	x		540
S21U			880	Top	x		430
S22U			710	Middle	x		600
S23U			930	Top	x		460
S24U			810	Top	x		540
S25U			930	Top	x		460
S26U			1010	Bottom	x		540
S27U			940	Top	x		420
S28U			800	Top/Middle	xxx		750/750/680
S29U*			920	Bottom/Middle	x		520
S30U			700	Top/Middle	x		540

TABLE I - continued

Shell No.	Chord (in.)	Perimeter (pct)	Buckle Load(lb)	Buckle Data Location	Snap	Soft	Falloff Load
			GROUP 2 (Cont'd)				
S31U			860	Top/Middle	x		500
S32U			810	Top		x	520
S33U			760	Top/Middle	x		620
S34U			910	Top	x		680
S35U			890	Top	x		600
S36U			900	Middle	xxx		820/720/500
S37U*			990	Bottom	x		500
S38U			940	Top	x		460
S39U			990	Top	x		520
S40U			990	Top	x		440
			GROUP 3 (10)				
S51U	2-1/4	.67	1120	Top/Middle	x	x	780
S52U			1020	Top		x	680
S53U			1310	Top	x		580
S54U			1100	Top	x		540
S55U			1390	Top	x		600
S56U			1210	Top	x		630
S57U			1110	Top	x		740
S58U			1260	Top	x	x	780
S59U			1220	Top/Middle	x		1110
S60U			1050	Top/Middle	x		-
			GROUP 4 (25)				
S61U	1-1/8	.86	1410	Top/Middle	x		900
S62U			1680	Top/Middle	x		830
S63U			1540	Top/Middle	x		900
S64U*			1800	Top/Middle	x		1020
S65U			1790	Top	x		760
S66U			1730	Top	x		660
S67U			1560	Top	x		640
S68U*			1690	Top/Middle	x		760
S69U			1710	Top	x		740
S70U			1620	Middle	x		1060
S71U			1360	Top	x		800
S72U			1500	Top/Middle	x		960
S73U*			1590	Middle	x		960
S74U			1470	Top	x		780
S75U			1460	Middle	x		1280
S76U			1300	Top/Middle	x		800
S77U			1630	Top	x		820
S78U			1450	Top	x		740
S79U			1200	Top	x		740
S80U			1400	Top/Middle	x		840

TABLE I - continued

Shell No.	Chord (in)	Perimeter (pct)	Buckle Load (lb)	Buckle Data			Falloff Load
				Location	Snap	Soft	
			GROUP 4 (Cont'd)				
S81U			1510	Top/Middle	x		780
S82U			1500	Top	x		740
S83U			1520	Top	x		760
S84U			1540	Top	x		700
S85U			1270	Top/Middle	x		740
			GROUP 5 (2)				
S86U	0	0	160			x	-
S87U	0	0	180		x		-

* Excellent Buckle Pattern

TABLE II. TWO-PLACE SYMMETRICAL DISTRIBUTED LOADING - TYPE A
Test Machine: 60,000-lb Tinius-Olsen
(See Figure 11)

Shell No.	Width	Buckle Load	Buckle Data Location	Snap	Soft	Falloff Load
			GROUP 1 (10 Tests)			
S103a	1	580	Top	x		200
S104a		580	Top/Bottom	x		-
S105a		530	Top	x		320
S106a		470	Top	x		340
S107a		500	Top		x	380
S108a		490	Top		x	390
S109a		480	Top		x	360
S70		600	Top		x	-
S71		480	Top/Middle	x		-
S72		500	Top/Middle		x	-
			GROUP 2 (50)			
S80a	1-7/8	1020	Top	x		580
S81a		1100	Middle	x		720
S82a		960	Top	x		500
S83a		1040	Bottom	x		730/520
S84a		980	Top	x		520
S85a		1040	Top	x		520
S86a		1020	Bottom	x		790
S87a		1020	Top		x	560
S88a		810	Top/Middle	x	x	660
S89a		990	Top/Middle	x		700
S90a		820	Top	x		660
S91a		1020	Top	x		540
S92a		1010	Top		x	600
S93a		840	Top	x		500
S94a		1010	Top	x		570
S95a		910	Middle	x		800
S96a		920	Bottom/Middle	x		780
S97a		800	Middle	x		760
S98a		1100	Top	x		660
S99a		980	Top	x	x	600
S100a		950	Middle	x		860/710
S101a		1010	Top/Middle	xx		960/670
S102a*		990	Middle			690
S80b		1080	Top	x		550
S81b		1120	Top/Middle	x		640
S82b		1070	Top	x		580
S83b		950	Top	x		600
S84b		1090	Top	x		600

TABLE II - continued

Shell No.	Width	Buckle Load	Buckle Data Location	Snap	Soft	Falloff Load
			GROUP 2 (Cont'd)			
S85b		1220	Top	x		580
S86b		980	Middle	x		800
S87b		1110	Top	x		640
S88b		1130	Top	x	x	660
S89b		1030	Top			600
S90b		1180	Top	x		640
S91b		1170	Top/Middle	x		700
S92b*		1220	Top/Middle	x		680
S93b		860	Top/Middle	x		620
S94b		1120	Bottom	x		900
S95b		970	Top	x		840
S96b		890	Top		x	600
S97b		1120	Top/Middle	x		700
S98b		1080	Top	x		620
S99b		910	Bottom/Middle	x		740
S100b		1090	Top	x		580
S101b		1150	Top	x		620
S102b		1090	Top	x		600
S103b*		1050	Bottom/Middle	x		900
S104b		1170	Top	x		600
S73		980	Top	x		-
S74		1010	Top		x	-
			GROUP 3 (10)			
S70a	2-7/16	1310	Top	x		-
S71a		1570	Bottom	x		1120
S72a		1420	Top	x		780
S73a		1440	Top	x		760
S74a		1390	Top	x		780
S75a		1400	Bottom	x		1120
S76a		1380	Top/Middle	x		980/850
S77a		1420	Top	x		1200/840/720
S78a		1470	Top	x		780
S79a		1420	Top	x		900

* Excellent Buckle Pattern

TABLE III. THREE-PLACE SYMMETRICAL DISTRIBUTED LOADING - TYPE A
Testing Mechine: 60,000-lb Baldwin-Lima-Hamilton
(See Figure 12)

Shell No.	α	Buckle Load	Buckle Data			Falloff Load
			Location	Snap	Soft	
			GROUP 1 (3 Tests)			
S21	40°	950	Top	x		-
S22		880	Top		x	-
S23		770	Top		x	-
			GROUP 2 (27)			
S55a	60°	970	Middle	x		-
S56a		1090	Bottom	x		-
S57a		990	Middle	x		-
S58a		1180	Top	x		-
S59a		1120	Bottom/Middle	x		-
S55b		1170	Top	x		700
S56b		1000	Bottom/Middle	xx		860/700
S57b		890	Top/Middle	x		520
S58b*		1000	Top/Middle	xx		900/800
S59b		1090	Top		x	850
S60b		990	Middle	x		680
S61b		1050	Top/Middle	xx		960/880
S62b*		1200	Top/Middle	x		760
S63b		1100	Top	x		680
S64b		1050	Top	x		680
S65b		880	Top	x		600
S66b		1190	Top	x		740
S67b		1100	Bottom	x		720
S68b		1010	Top	x		820
S69b		1070	Top	x		940
S70b		880	Top		x	760
S71b		910	Top	x		700
S72b		1040	Top/Middle	xx		980/760
S73b		1020	Top	x		850
S74b		890	Top/Middle	x		660
S75b		1000	Top/Middle	x		860
S76b		1100	Bottom/Middle	x		740
			GROUP 3 (26)			
S60c	100°	1520	Top/Middle	x		-
S61c		1430	Top/Middle	x		-
S62c		1370	Top/Middle	x		-
S63c		1860	Top/Middle	x		-
S64c		1540	Top/Middle	x		-
S60c		1670	Top/Middle	x		620
S61c		1680	Top	x		840

TABLE III - continued

Shell No.	α	Buckle Load	Buckle Data Location	Snap	Soft	Falloff Load
			GROUP 3 (Cont'd)			
S62c		1610	Top/Middle	x		1140
S63c		1580	Top	x		1100
S64c		1700	Top	x		920
S65c		1540	Bottom/Middle	x		1360
S66c		1690	Top	x		1120
S67c		1800	Top/Middle	x		1060
S68c		1260	Bottom/Middle	x	x	-
S69c		1630	Middle	x		1380
S70c		1500	Top/Middle	x		1000
S71c		1680	Bottom/Middle	xx		1500/1260
S72c		1600	Top	x		-
S73c		1570	Top	x		1150
S74c		1600	Top	x		1180
S75c		1760	Top	x		860
S76c		1660	Top	x		1200
S77c		1640	Top/Middle	x		1210
S78c		1680	Top	x		1200
S79c		1620	Top	x		1020
S80c		1890	Top/Middle	x		1160
			GROUP 4 (3)			
S24	80°	1290	Top	x		-
S25		1120	Top	x		-
S26		1220	Top		x	-

* Excellent Buckle Pattern

TABLE IV. TWO-PLACE SYMMETRICAL DISTRIBUTED LOADING - TYPE B
Testing Machine: 60,000-lb Tinius-Olsen
(See Figure 13)

Shell No.	Width	Buckle Load	Buckle Data Location	Snap	Soft	Falloff Load
			GROUP 1 (3 Tests)			
S56	1"	685	Bottom	x		-
S57		745	Bottom	x		-
S58		800	Bottom	x		-
			GROUP 2 (53)			
100	1-7/8"	1110	Top/Bottom			800
101		1000	Bottom/Middle			750
102		1020	Top/Middle			730
103		1155	Top			800
104		1025	Upper 1/3			725
105		1240	Top			930
106		940	Top/Middle			550
107		1125	Top/Bottom			690
108		1170	Middle			720
109		1055	Top			830
110		1080	Top/Middle			740
111		1110	Top			900/810
112		950	Bottom/Middle			700
113		970	Top			700
114		1200	Top/Bottom			860
115		1100	Top/Low 1/3			670
116		1035	Top/Bottom			600
117		1240	Bottom/Middle			1070
118		1105	Top			730
119		955	Top/Upper 1/3			700
120		980	Top			690
121		1155	Top			630
122		1160	Top			800
123		1130	Top			700
124		1105	Top			730
125		1000	Top			700
126		1090	Top			720
127		1065	Top/Middle			940
128		1045	Top/Upper 1/3 and Bottom			800
129		1250	Top			740
130		970	Top/Middle 1/3			550
131		1145	Top			550
132		1140	Middle			740
133		970	Top			690
134		1155	Top			650
135		1150	Bottom/Lower 1/3			550

TABLE IV - continued

Shell No.	Width	Buckle Load	Buckle Load Location	Snap	Soft	Falloff Load
			GROUP 2 (Cont'd)			
136		1050	Bottom			550
137		990	Top/Upper 1/3			620
138		1265	Top			820
139		915	Top/Middle 1/3			650
140		1070	Top/Bottom			790
141		935	Top			680
142		1175	Top			740
143		895	Top			700
144		980	Top/Upper 1/3			760
145		1015	Top			760
146		1085	Top			650
147		1115	Top			720
148		1160	Top			720
149		1050	Top			730
S53		1110	Top			-
S54		1165	Top			-
S55		1140	Bottom			-
			GROUP 3 (25)			
150	2-7/16	1650	Top/Bottom	x		1200/980
151		1710	Top	x		960
152		1730	Top	xxxx		1060/980/900/760
153		1790	Top/Middle	xxxxx		1100/1080/1010/900/800
154		1550	Top/Middle	xx		880/700
155		1570	Top	x		1000
156		1720	Middle	xx		1260/1000
157		1510	Top	x		1100
158		1620	Top	x		880
159		1560	Top	x		900
160		1560	Top/Middle	x		1100
161		1540	Top/Middle	x		950
162		1830	Top	x		1040
163		1550	Top		x	900
164		1580	Top	x		1000
165*		1670	Top	x		900
166		1610	Top	x		920
167		1620	Top/Middle	x		1200
168		1430	Top		x	-
169		1510	Top		x	1000
170		1430	Top/Middle	x		1020
171		1540	Top	x		1000
S50		1535	Top	x		-
S51		1500	Top		x	-
S52		1790	Top	x		-

* Excellent Buckle Pattern

TABLE V. THREE-PLACE SYMMETRICAL DISTRIBUTED LOADING - TYPE B
Testing Machine: 60,000-lb Baldwin-Lima-Hamilton
(See Figure 14)

Shell No.	α	Buckle Load	Buckle Data Location	Snap	Soft
		GROUP 1 (4 Tests)			
S1a	18°	620	Top	x	
S2a		520	Top	x	
S3a		590	Middle	x	
S4a		610	Top	x	
		GROUP 2 (11)			
S16a	40°	970	Top	x	
S17a		800	Middle	x	
S18a		1000	Top 1/3	x	
S19a		800	Bottom/Middle	x	
S20a		960	Top	x	
S21a		990	Top	x	
S22a		760	Bottom/Middle	x	
S23a		950	Top	x	
S1		940	Top	x	
S2		1000	Top	x	
S3		1030	Top	x	
		GROUP 3 (9)			
S5a	60°	1020	Bottom/Middle	x	
S6a		1130	Bottom/Middle	x	
S7a		1060	Top	x	
S8a		1080	Top	x	
S40a		1280	Top	x	
S41a		1130	Bottom/Middle	x	
S42a		920	Middle	x	
S43a		1230	Top/Middle	x	
S44a		1050	Middle	x	
		GROUP 4 (11)			
S24a	80°	1500	Top	x	
S25a		1360	Bottom/Middle	x	
S26a		1320	Bottom/Middle	x	
S27a		1400	Top	x	
S28a		1300	Bottom	x	
S29a		1260	Top	x	
S30a		1340	Top	x	
S31a		1300	Top	x	
S4		1280	Top	x	
S5		1060	Top		
S6		1150	Top	x	

TABLE V - continued

Shell No.	α	Buckle Load	Buckle Data Location	Snap	Soft
		GROUP 5 (7)			
S9a	100°	1640	Top/Middle	x	
S10a		1410	Top/Middle	x	
S11a		1820	Middle	x	
S12a		1840	Top/Middle	x	
S13a		1940	Top/Middle	x	
S14a		1440	Top/Middle	x	
S15a		1800	Top/Middle	x	
		GROUP 6 (10)			
S32a	120°	1920	Top	x	
S33a		1620	Top	x	
S34a		1690	Top	x	
S35a		2060	Top/Middle	x	
S36a		2080	Top	x	
S37a		1730	Top	x	
S38a		2070	Top	x	
S7		1960	Top	x	
S8		1660	Top	x	
S9		1760	Middle	x	

DISCUSSION OF THE RESULTS OF THE FIRST SERIES

Reference is made to the information contained in Figures 16 through 18. The quality of the data is seen to be high. The standard deviations vary from 6 percent at the high load levels, which correspond to the greater loaded areas, to 12 percent for loading over a smaller fraction of the circumference. This variation is well inside that frequently experienced. Mossakovskii and Smelyi,[12] for instance, quote 15 percent as being not unreasonable.

The data of Figure 19, which encompass all load distribution for the type A conditions, are strong evidence that the critical stress which causes instability is independent of the nature of the end load distribution. Statistical treatment and normal correlation procedures outlined in the appendix indicate that the straight line σA represents this material to a confidence level of 95 percent. The results depicted in Figure 20 are totally consistent with those referred to above.

THE SECOND SERIES OF TESTS

In the second series of tests, the specifications were much broader than those for the first series. Previously, only the application of classic procedures to determine the influence of nonuniformity of stress conditions was of any concern. Preparations had been made to use, if necessary, a very large number of specimens and to accept the time-consuming process of setting up and testing these specimens, whereas in this series the use of a single specimen to develop a procedure for studying the quality of the test vehicle and at the same time to study the influence of combined compression and flexure on the buckling characteristics of thin-walled structures was desired. The study was begun with the observation taken from the first series; namely, that when a cylindrical shell is loaded with discrete loads around its circumference, the buckling which takes place occurs in regions which are closely associated with the loaded region. Therefore, there must be a greater tendency to buckle in some regions of the shell than in others if a cylindrical shell is loaded by an offset load. Thus, the shell can be considered in a slightly different light. The regions which tend to buckle can be considered to be plates with undetermined, but nevertheless repeatable, loading and support conditions for all similar overall load application conditions. Hence, a single shell can, under these conditions, be looked upon as a wide population of test vehicles, each of which bears some connection with every other similar specimen. Clearly, the methods of manufacture of the shell must mean that individual elements, cut at random around the periphery, would differ from each other with respect to the quality. Thus, it seems reasonable to consider that a circular traverse would provide information relative to the quality of the shell in regions which are defined as lengthwise strips. Experience with pure compressional buckling would indicate that if the buckle load is defined as that load which produces maximum buckle generation, then each strip would have the same load; but the kurtosis of the buckle distribution curve would alter with quality, becoming more platykurtic with improved quality. In other words, a good section would tend to buckle uniformly all over at one and the same time.

Thus, in the first tests of the second series, the circular traverse method was investigated as a technique for quality control. The second tests of the series were made to determine the influence of combined compression and flexure on the buckling characteristics of thin-walled circular cylindrical shells. The case when the offset of load was zero, as closely as could be determined, was used to check the quality control procedure.

TEST SPECIMENS

The specimen used in these tests was manufactured in the laboratory by the following procedure. A thick-walled tube of appropriate dimension and specification was accurately bored and honed. It was then carefully turned until the wall thickness was of the order of 1/32 inch. When this was complete, the shell was shrunk onto an accurate mandrel whose coefficient of linear expansion differed from that of the shell material. The mandrel-shell combination was then turned between centers, using a carbide tool, until the final chosen thickness was approximated. The final dimension was achieved by lapping and polishing.

The shell so manufactured was assembled in loading heads and was made "encastré" in the loading heads with a low-melting-point alloy. A buckle depth-restricting mandrel was arranged inside the shell, concentric with the shell. A gap of approximately 1/8 inch was allowed between the head of the mandrel and the lower face of the upper loading plate. A small hole permitted entrapped air to escape when the shell volume was reduced by the buckle formation.

TEST PROCEDURE

The cylindrical shell manufactured in accordance with the test specimens in the preceding section was tested in a 60,000-pound-capacity Tinius-Olsen Universal test machine under combined flexure and compression. In order to make the setup process as convenient as possible, a special jig was devised. Details of this are shown in Figure 21. To assemble the test specimen in the machine, the following procedure was adopted. The special jig was located on the loading platform, and the lower loading ball was positioned. Next, the test specimen was aligned on the jig, being supported in the unloaded state by the three low rate springs seen in Figure 21. The top loading ball was now sited in the correct place, and the machine head lowered until contact was made with the ball. By paying particular attention to detail, and by checking and rechecking, it was found possible to align the upper and lower loading balls vertically with great accuracy.

For the first tests made, the line of action of the applied load was kept at a constant distance Δ from the axis of the shell, such that $\Delta/r = 3/8$. Eight positions, 45 degrees apart, were used. A buckle number load history was determined for each loading station.

The next tests in this series were repeats of this first family except that Δ/r was changed to 1/2.

The final tests were conducted using a radial traverse instead of the circular traverse used for the first and second families of the series. In this radial traverse, seven values of Δ/r were used.

The cylinder, as set in the machine for testing, is seen in Figure 22.

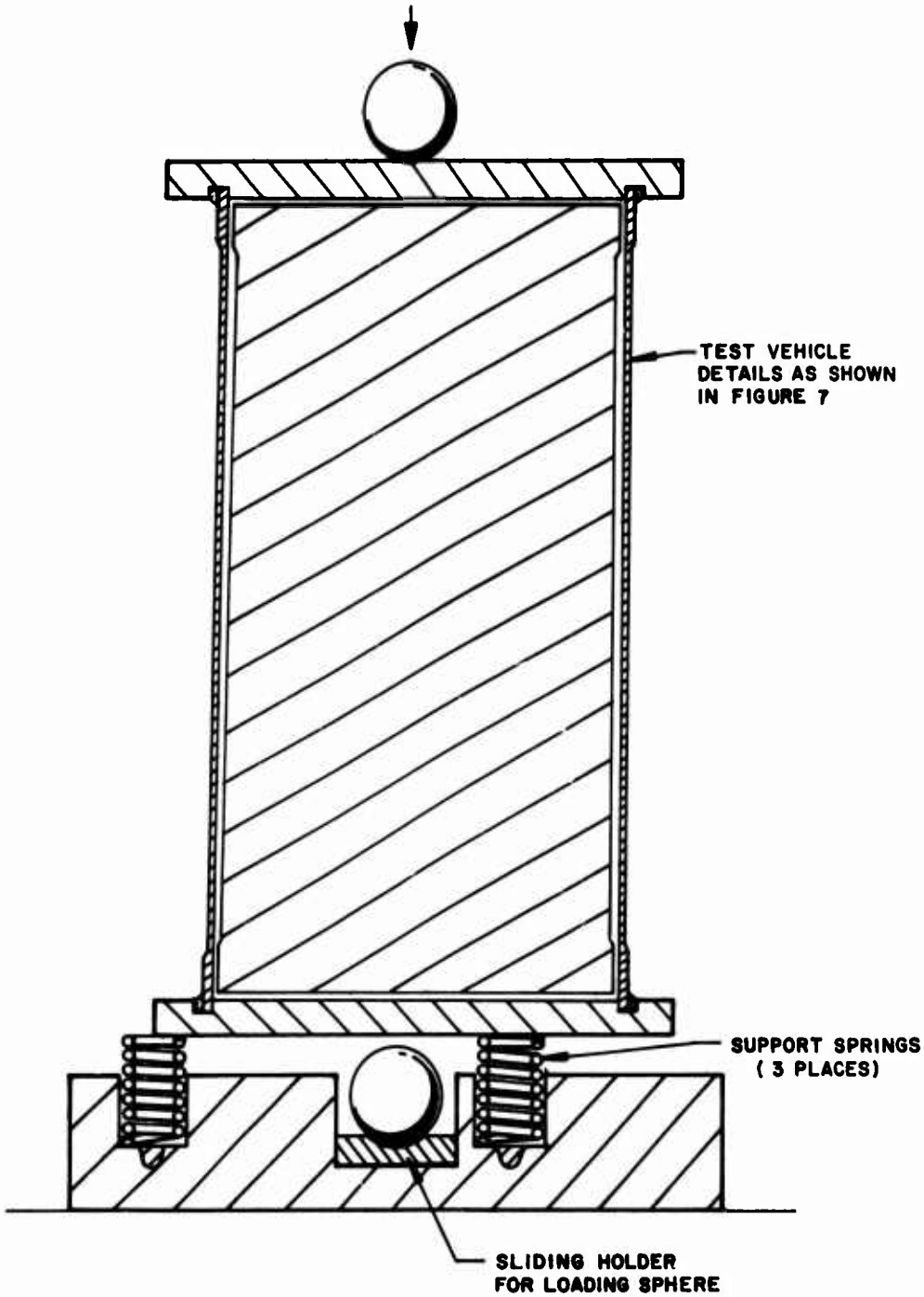

Figure 21. Cross Section of Series 2 Test Vehicle With Restraining Mandrel and Testing Jig.

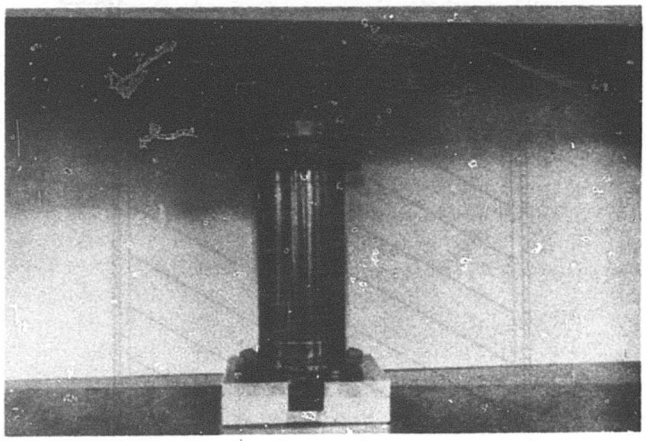

Figure 22. Series 2 Test Vehicle and Loading Jig in Testing Machine.

DISCUSSION OF THE RESULTS OF THE SECOND SERIES

The mechanical properties of the material of the test cylinder are given in Figure 23. The results of the first circular traverse with $\Delta/r = 3/8$ are given in Table VI and are presented in graphical form in Figure 24. The buckle number load histories displayed therein follow normal cumulative distributions. The buckle load for each section, defined as the load for maximum buckle germination, is substantially constant. The variation which does occur is so slight that it must be considered to be accidental. It is seen that the main difference among the several data presented is that at one station the standard deviation is very large relative to the value of this parameter at all other stations. This implies, then, that perhaps this section should be the weakest section of the shell or at least the section with the greatest irregularity.

The results of the second circular traverse with $\Delta/r = 1/2$ are also presented in Table VI and are displayed graphically in Figure 25. The results are in 1:1 correspondence with those previously obtained.

Figure 26 shows the variation in buckling load for the circular traverse at 3/8r and 1/2r eccentricities. The tendency toward a constant value for any radial position of the load is clearly seen.

In Figure 27 the variation in standard deviation for these two families of tests is given as a function of the angular position of the test load. It is immediately apparent that the maximum values of σ are located in the same regions.

The shell was now tested with $\Delta/r = 0$, i.e., under pure axial compression. The area of first buckling under these conditions was found to correspond to part of the region for which the maximum value of standard deviation was measured. The results of testing under pure axial compression are given in Table VII. These are the data used to plot the example curve shown in Figure 6.

If the hypothesis that initial imperfection determines the point of initial buckle germination is accepted, then the results given above indicate that:

1. Under identical load conditions, nominally identical specimens have the same buckle load, when this load is defined as the load which causes maximum buckle generation.
2. The kurtosis of the curve of rate of change of number of buckles as a function of load is a measure of the degree of imperfection.

For the final family of tests, the shell was set such that the defective region as determined by the above-described procedure lay in opposite quadrant to the radial traverse line. With the shell so located, a radial traverse was made using values of Δ/r from 0 to 3/4, in 1/8 steps. The buckle number load histories for these offsets are given in Tables VII and VIII and are illustrated graphically in Figures 28 and 29. The corresponding buckle patterns are shown in Figure 30. From these results it is

seen that in each case the buckle number load histories are normal cumulative distributions. It is observed that there is no change in the shape, size, or location of the buckles formed in the various cases, but that the size of the population varies with load location. The variation in population size as a function of offset magnitude is portrayed in Figure 31. It is clear from this curve that when Δ/r is greater than $1/5$, a very large percentage of the surface of the shell is devoid of buckles.

This observation suggests immediately the main advantage that might derive from the use of a radial traverse. It seems reasonable to conclude, bearing Saint Venant's principle in mind, that the same information might be obtained from an incomplete shell as can be obtained from a complete shell by use of the radial traverse procedure. It is pertinent to remark that if a seam is to be used, the location for it is clear and the procedure of offset loading is likewise justified.

The final results of the tests are given in Figure 32 - a curve of critical load versus offset distance. On this curve a "theoretical line" has been superposed, derived on the assumption that the stresses in the shell can be computed from

$$f_b = \frac{P}{A} + \frac{M}{Z} = \frac{P}{A}\left(1 + \frac{2\Delta}{r}\right) \qquad (2)$$

and from the hypothesis that $f_b = f_{cr}$ = a constant for a given shell when buckled. The agreement between the observed and the "predicted" is remarkable. Thus, it is concluded from the second family of tests that a cylindrical shell under combined flexure and compression buckles when the compressive stress reaches a level which would have initiated buckling under pure axial compression.

This result is in agreement with the result of Seide and Weingarten but in disagreement with that of Flügge. However, it is only fair to point out that Flügge qualifies his result by defining a buckle aspect ratio, but this ratio does not appear to occur in practice.

The stress obtained as the critical value for the cylinder under pure axial load is only slightly lower than that given by the classic formula

$$\sigma = 0.605\,\frac{Et}{r} \qquad (3)$$

The variation is not sufficient to discredit this formula or to justify Fischer's value of $0.065 \times 0.605\ Et/r$. It is the normal inaccuracy due to operator and equipment error.

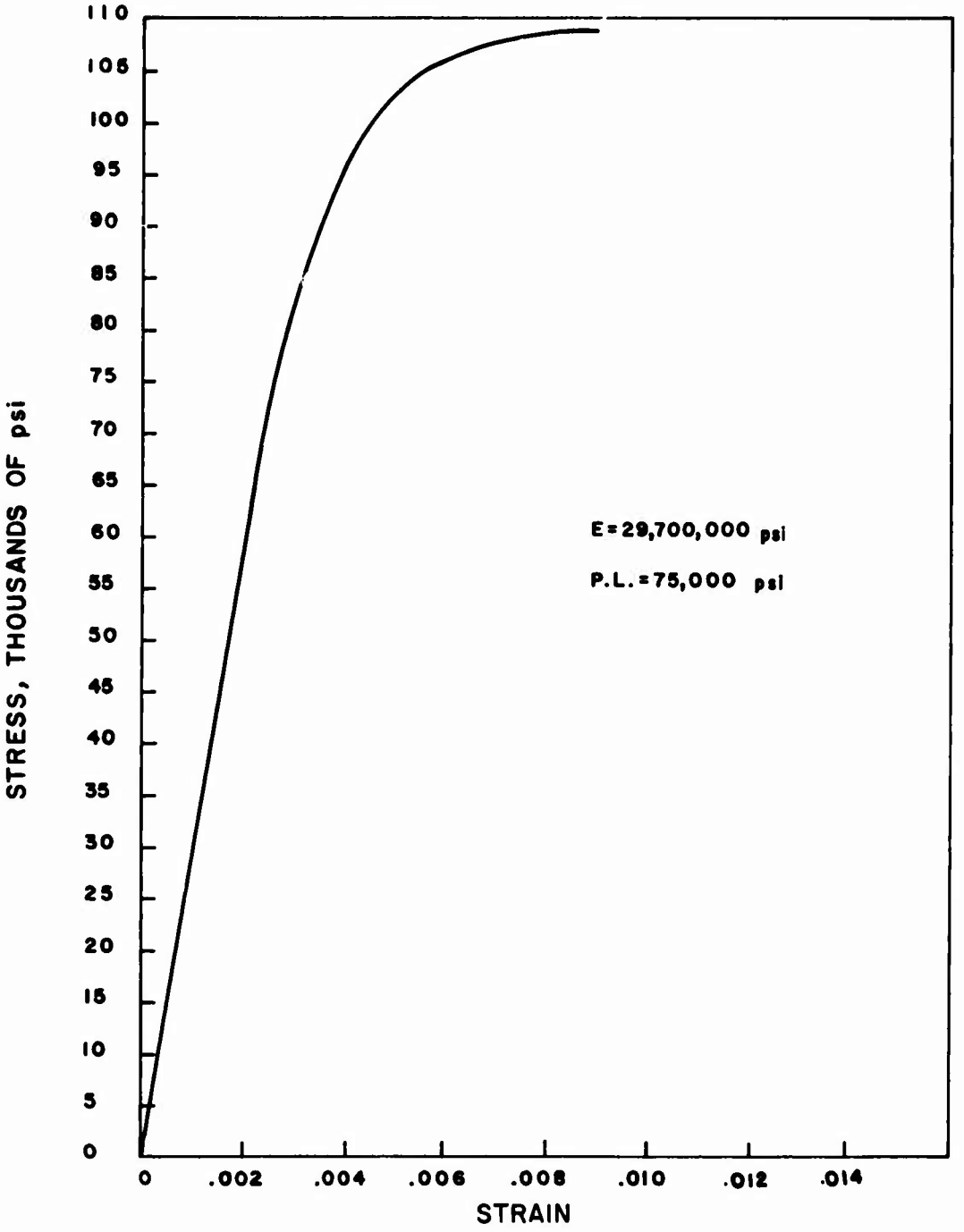

Figure 23. Stress-Strain Curve for Material of the Series 1 Test Specimen.

TABLE VI. CIRCULAR TRAVERSE OF LOADING FOR THE SHELL SPECIMENS OF SERIES 2 TESTS

Buckle Count vs Load for Eight Circular Positions

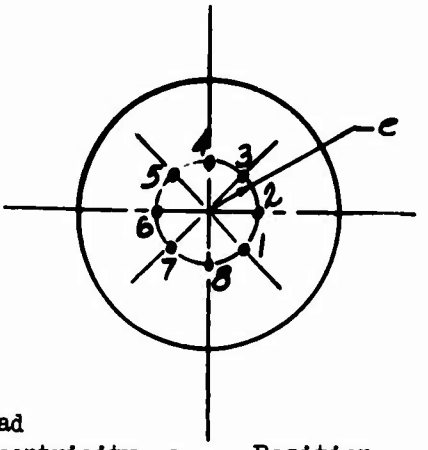

Specimen details given in Figure 7. Experimental set-up shown in Figures 21 and 22.

Load Eccentricity, e	Position	Load (lb)	Number of Buckles	Buckle Increment
3/8r	1	460	13	
		480	31	18
		500	59	28
		520	76	17
		540	82	6
	2	455	14	
		480	32	18
		500	53	21
		520	73	20
		540	82	9
	3	435	7	
		455	19	12
		475	37	18
		495	55	18
		515	70	15
		535	81	11
	4	435	12	
		455	23	11
		475	36	13
		495	48	12
		515	60	12
		535	70	10
		555	78	8
	5	445	14	
		465	23	9
		485	35	12
		505	58	23
		525	72	14
		545	81	9

TABLE VI - continued

Load Eccentricity, e	Postition	Load (lb)	Number of Buckles	Buckle Increment
3/8r	6	462	20	
		482	33	13
		502	53	20
		522	69	16
		542	80	11
	7	452	16	
		472	40	24
		492	51	11
		512	73	22
		532	84	11
	8	475	25	
		490	38	13
		505	58	20
		520	72	14
		535	82	10
		550	89	7
1/2r	1	400	3	
		420	26	23
		440	52	26
		460	70	18
		480	76	6
	2	400	7	
		420	23	16
		440	50	27
		460	70	20
		480	78	8
	3	385	6	
		405	19	13
		425	46	27
		445	69	23
		465	77	8
	4	370	6	
		390	24	18
		410	33	19
		430	50	17
		450	61	11
		470	69	8
	5	402	14	
		422	40	20
		442	58	18
		462	74	16
		472	80	6
	6	400	9	
		420	22	13
		440	48	26
		460	69	21
		480	76	7

TABLE VI - continued

Load Eccentricity, e	Position	Load (lb)	Number of Buckles	Buckle Increment
1/2r	7	395	11	
		415	35	24
		435	52	17
		455	66	14
		475	74	8
	8	390	4	
		410	11	7
		430	39	28
		450	64	25
		470	77	13

GRAPHIC REPRESENTATION OF THE DATA OF TABLE III NORMAL PROBABILITY COORDINATES.

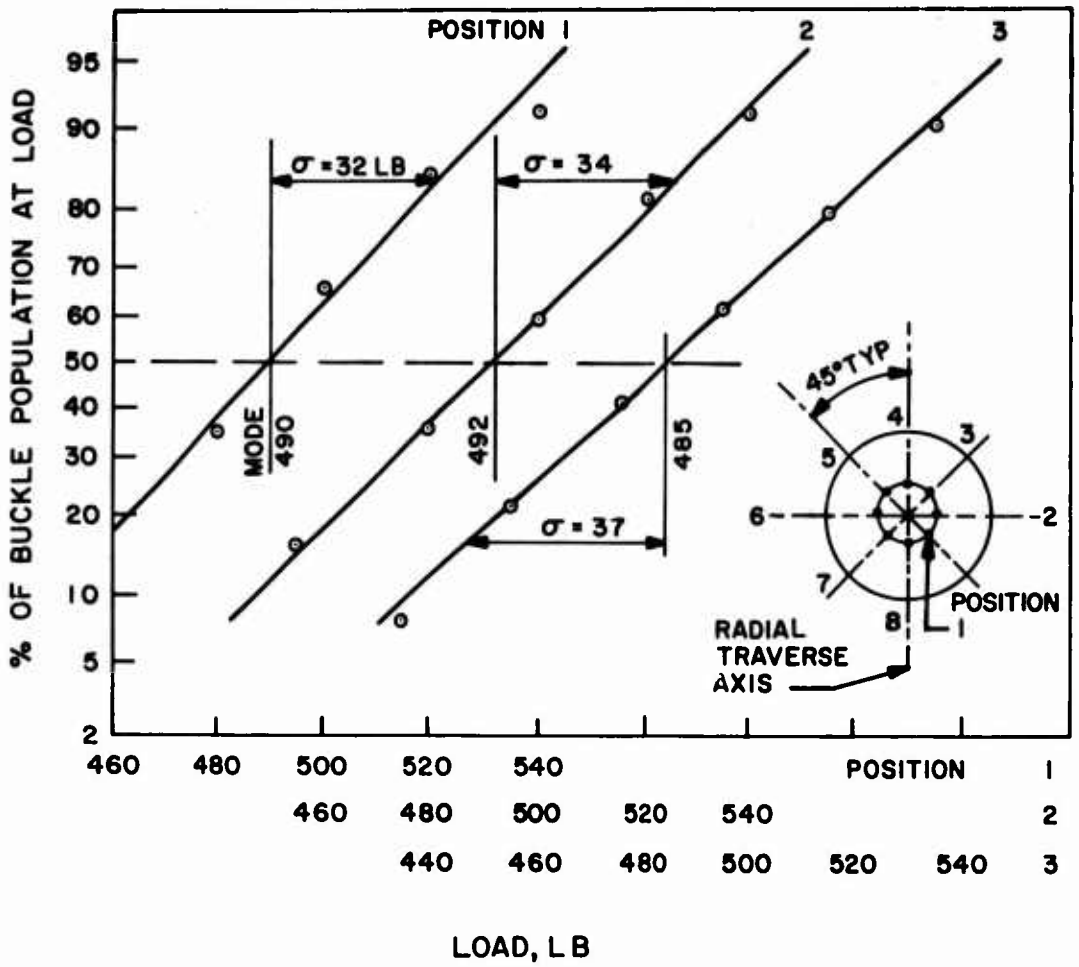

Figure 24. Results of Circular Traverse of Loading for the Shell Specimen of Series 2 Tests, Eccentricity of Load = 3/8r.

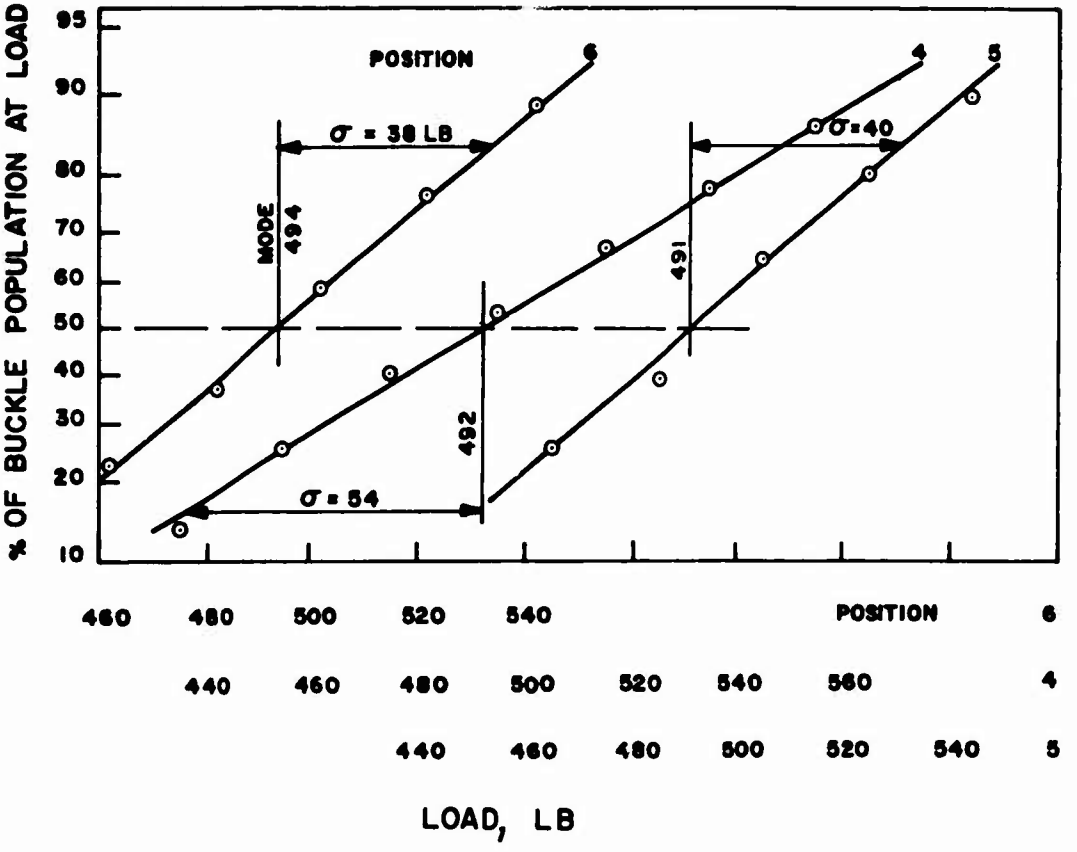

Figure 24. Continued.

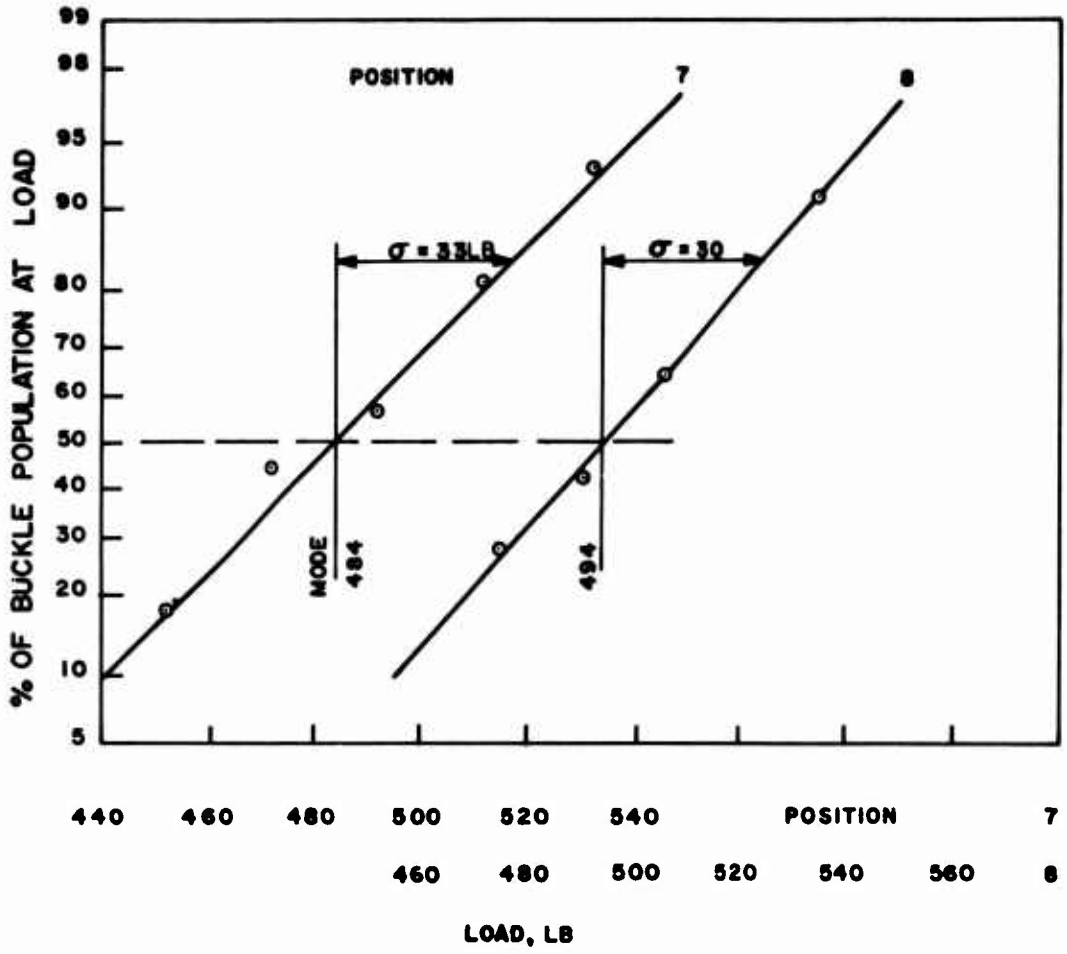

Figure 24. Continued.

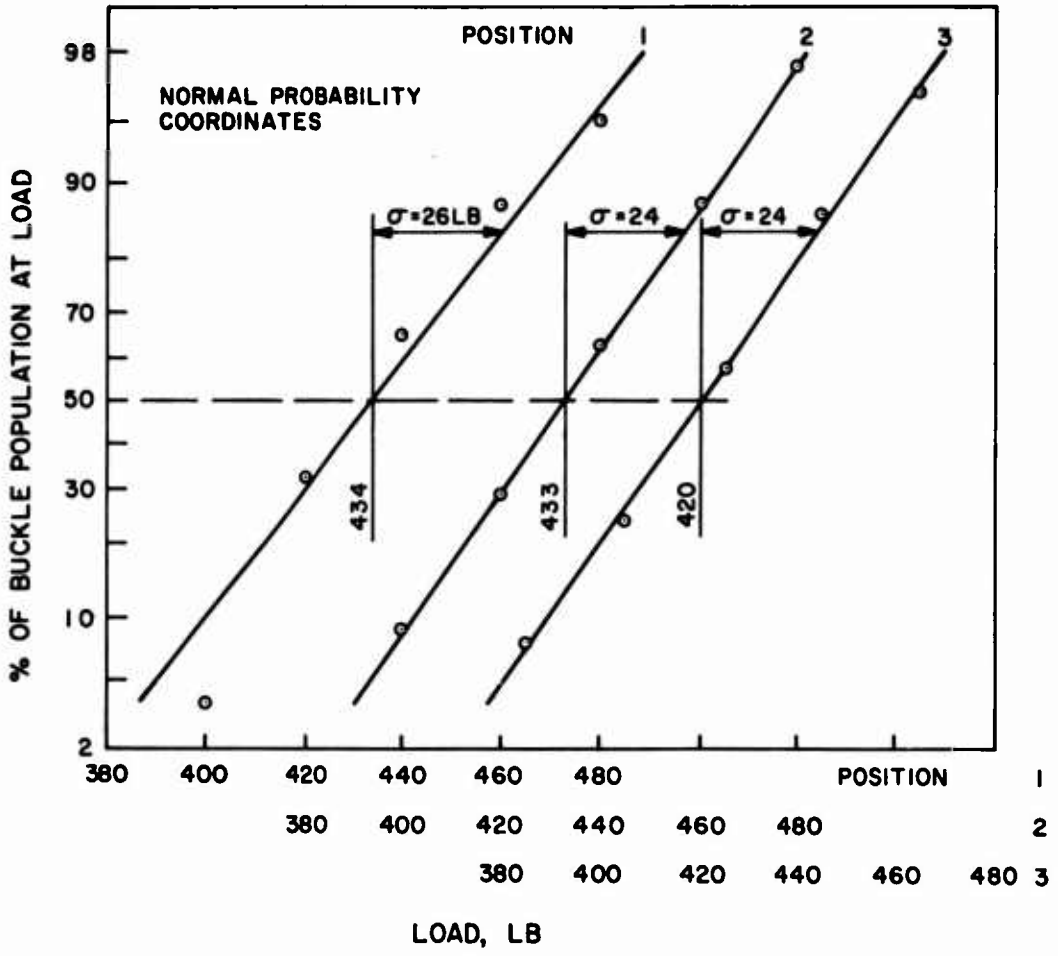

Figure 25. Results of Circular Traverse of Loading for the Shell Specimen of Series 2 Tests, Eccentricity of Load = 1/2r.

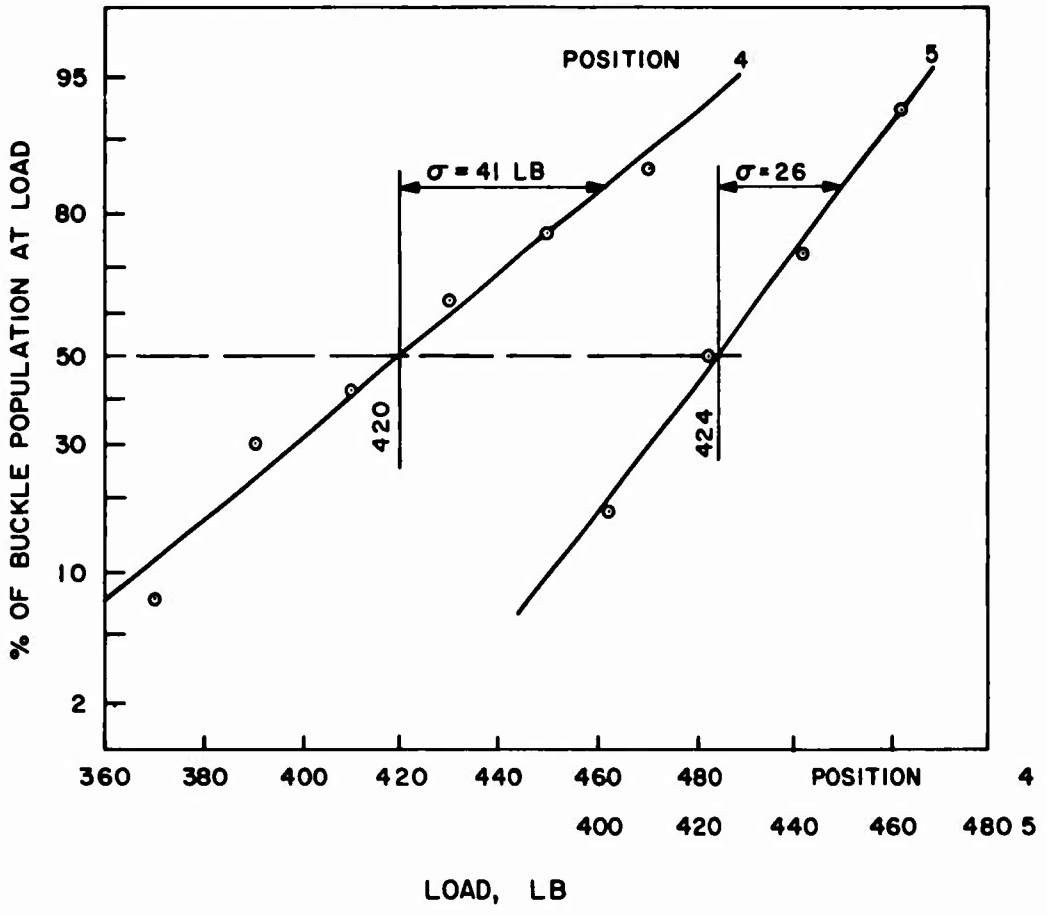

Figure 25. Continued.

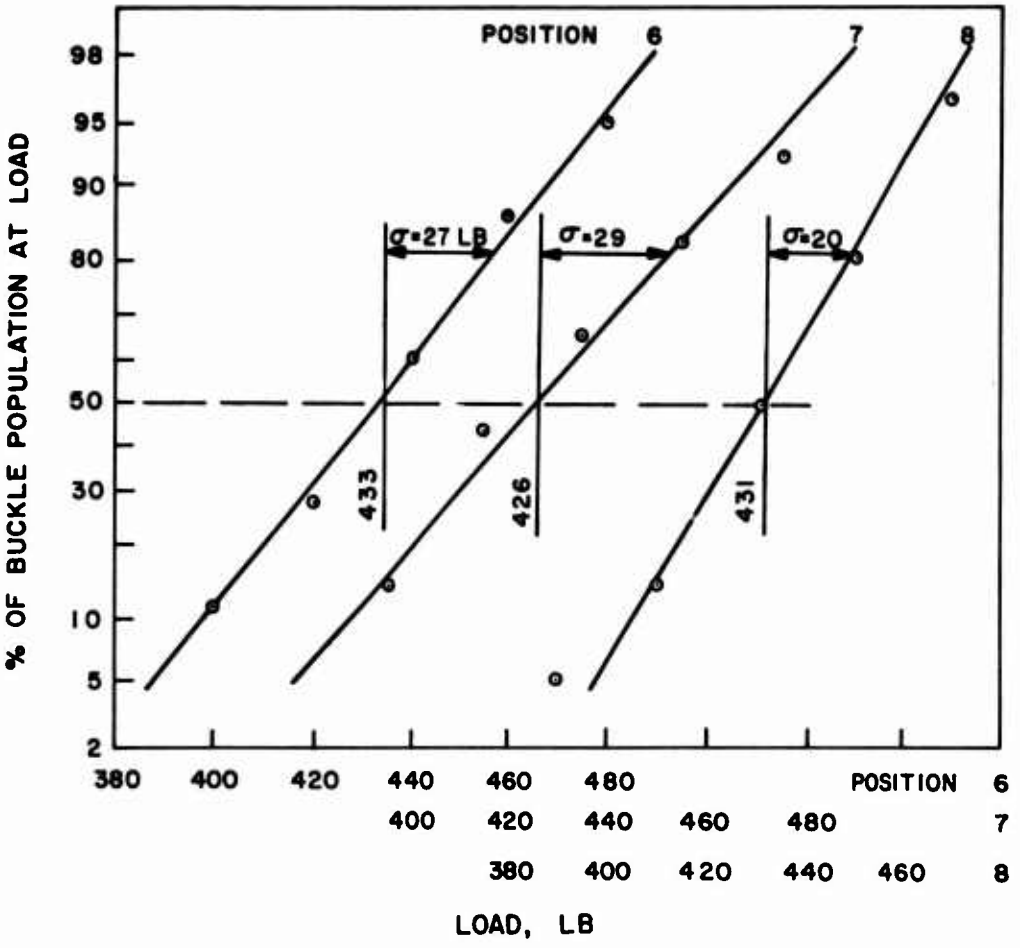

Figure 25. Continued.

BASIC DATA CONTAINED IN TABLE VI

DETERMINATION OF MODE VALUES FOR e = 3/8r IS ILLUSTRATED IN FIGURE 27

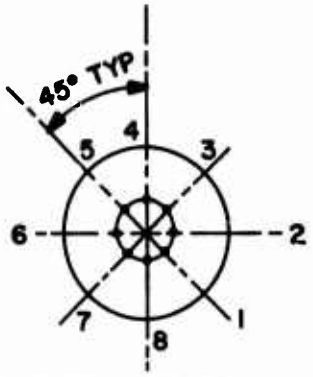

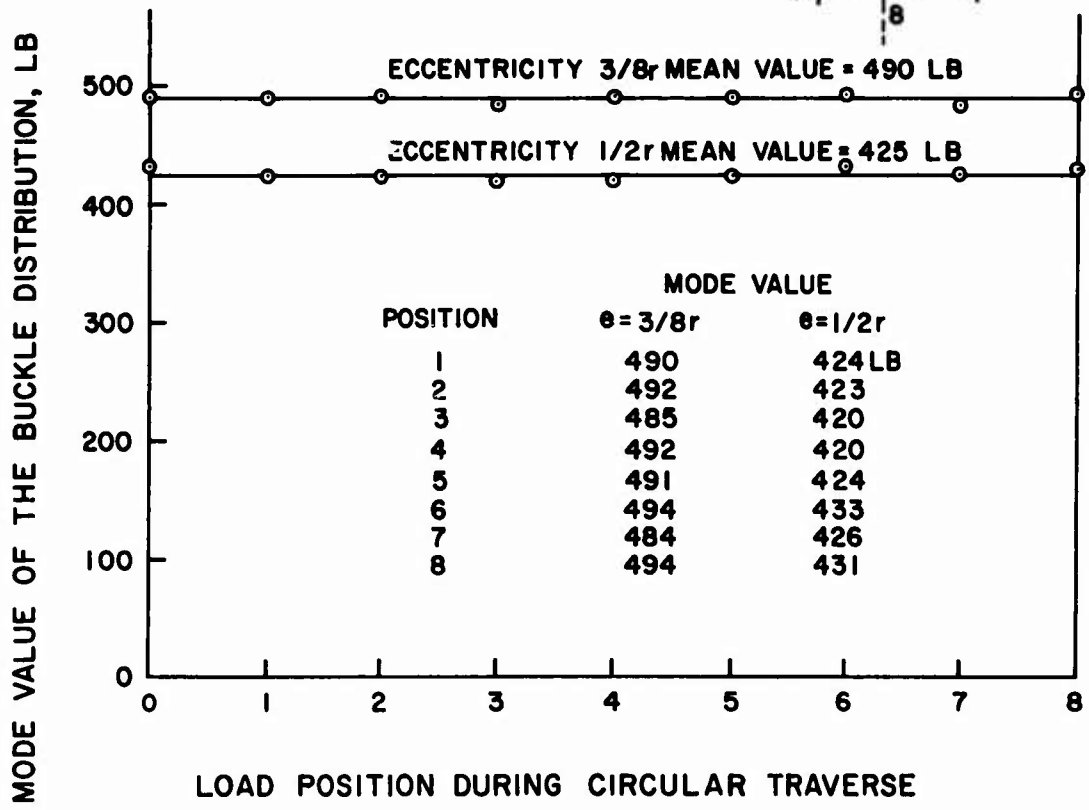

Figure 26. Maximum Buckling Rate Load for Eccentric Loading at Eight Equally Spaced Circular Positions.

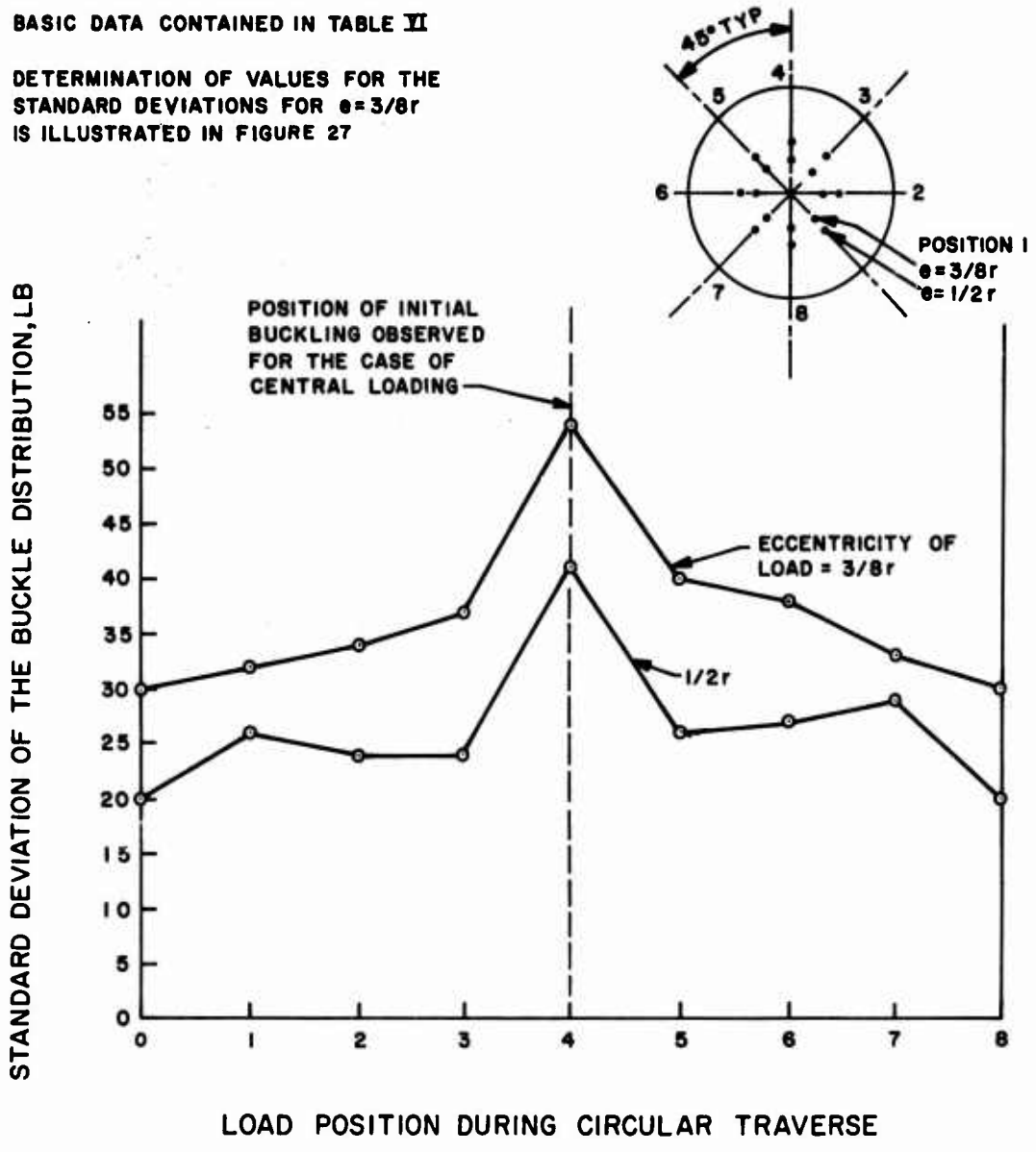

Figure 27. Initial Buckling Region of Shell Specimen of Series 2 Tests as Revealed by Circular Traverses of Loading.

TABLE VII. CENTRAL AXIS LOADING FOR THE SHELL SPECIMEN OF SERIES 2 TESTS

Buckle Count vs Load

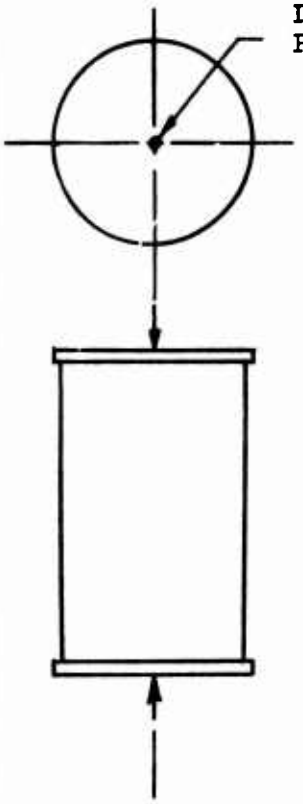

Load (lb)	Number of Buckles	Buckle Increment
740	82	
760	115	33
780	151	36
800	179	28
820	204	25
840	222	18
860	239	17

TABLE VIII. RADIAL TRAVERSE OF LOADING FOR THE SHELL SPECIMEN OF SERIES 2 TESTS

Buckle Count vs Load for Six Radial Stations

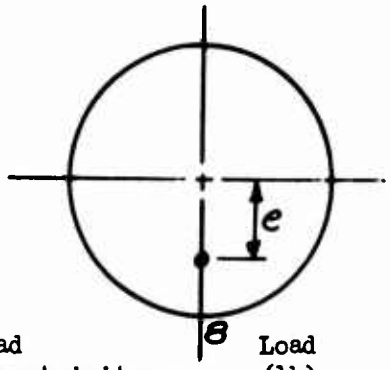

Specimen details given in Figure 7. Experimental setup shown in Figures 21 and 22.

Load Eccentricity, e	Load (lb)	Number of Buckles	Buckle Increment
1/8r	625	49	
	640	64	15
	650	77	13
	665	85	8
	685	99	14
	700	118	19
	730	131	13
	750	143	12
	780	151	8
	800	157	6
	820	170	13
	850	174	4
1/4r	540	16	
	560	36	20
	580	56	20
	600	84	28
	620	101	17
	640	106	5
3/8r	475	25	
	490	38	13
	505	58	20
	520	72	14
	535	82	10
	550	89	7
1/2r	410	11	
	420	26	15
	430	41	15
	440	57	16
	450	67	10
	462	77	10

TABLE VIII - continued

Load Eccentricity, e	Load (lb)	Number of Buckles	Buckle Increments
5/8r	340	4	
	360	13	9
	380	28	15
	400	43	15
	420	58	15
	440	69	11
3/4r	305	8	
	325	13	5
	350	34	21
	370	52	18
	390	64	12
	410	70	6

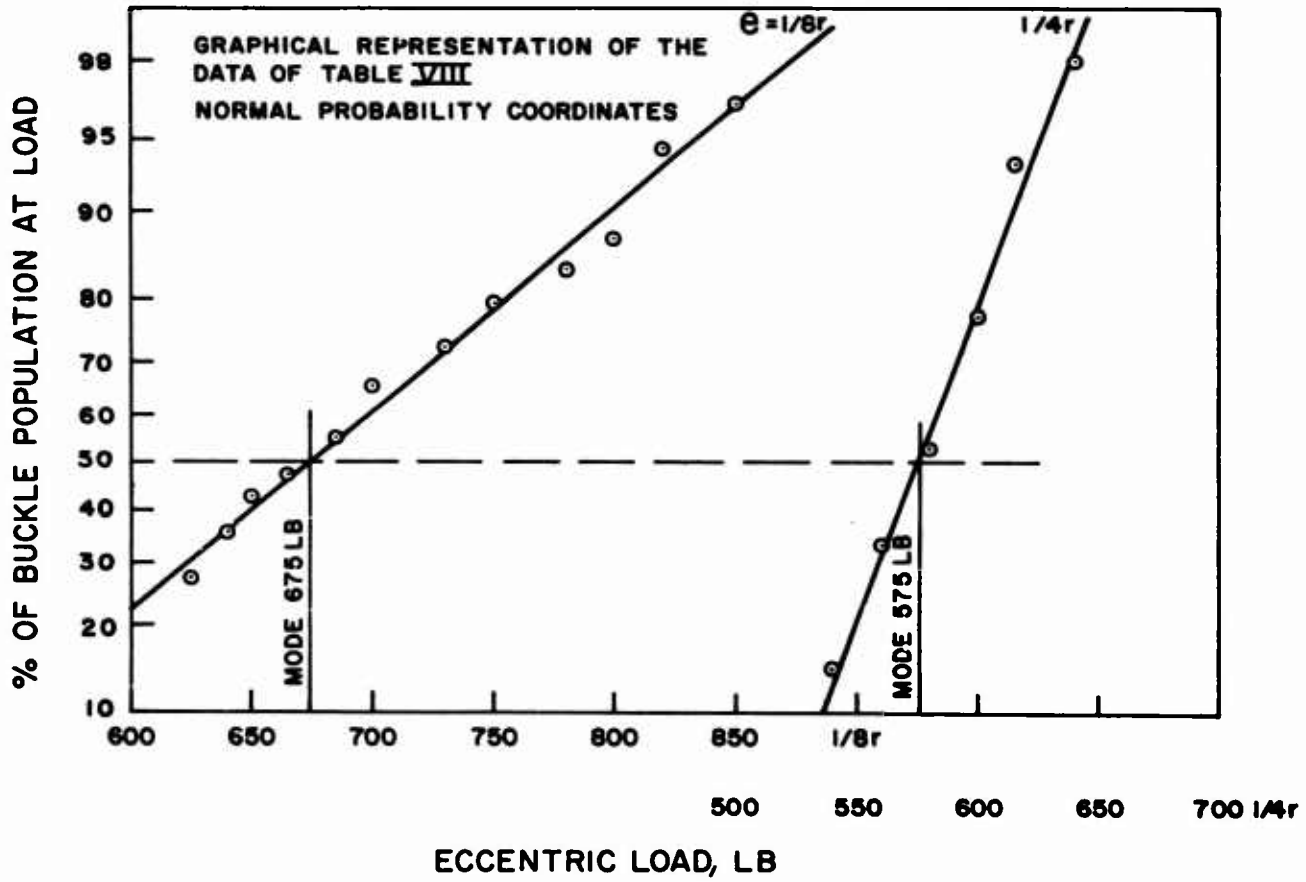

Figure 28. Results of Radial Traverse of Loading for the Shell Specimen of Series 2 Tests.

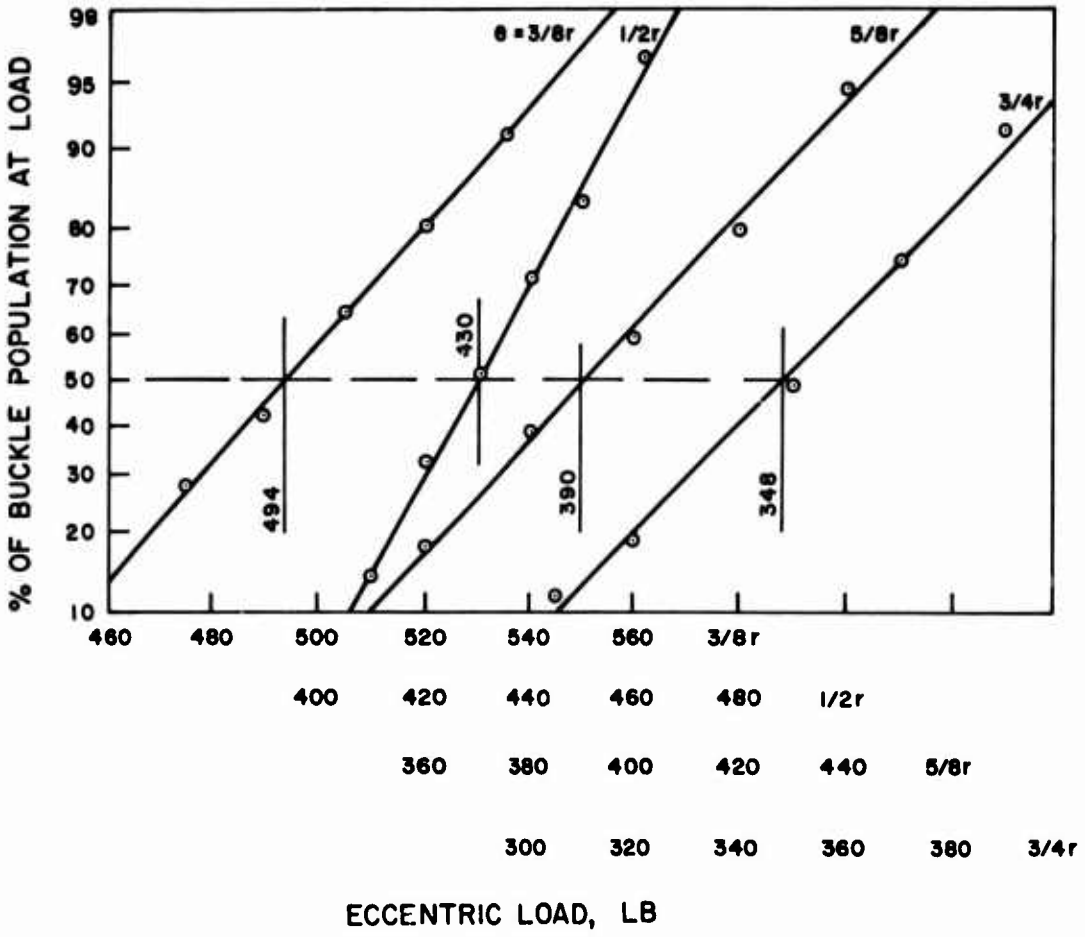

Figure 28. Continued.

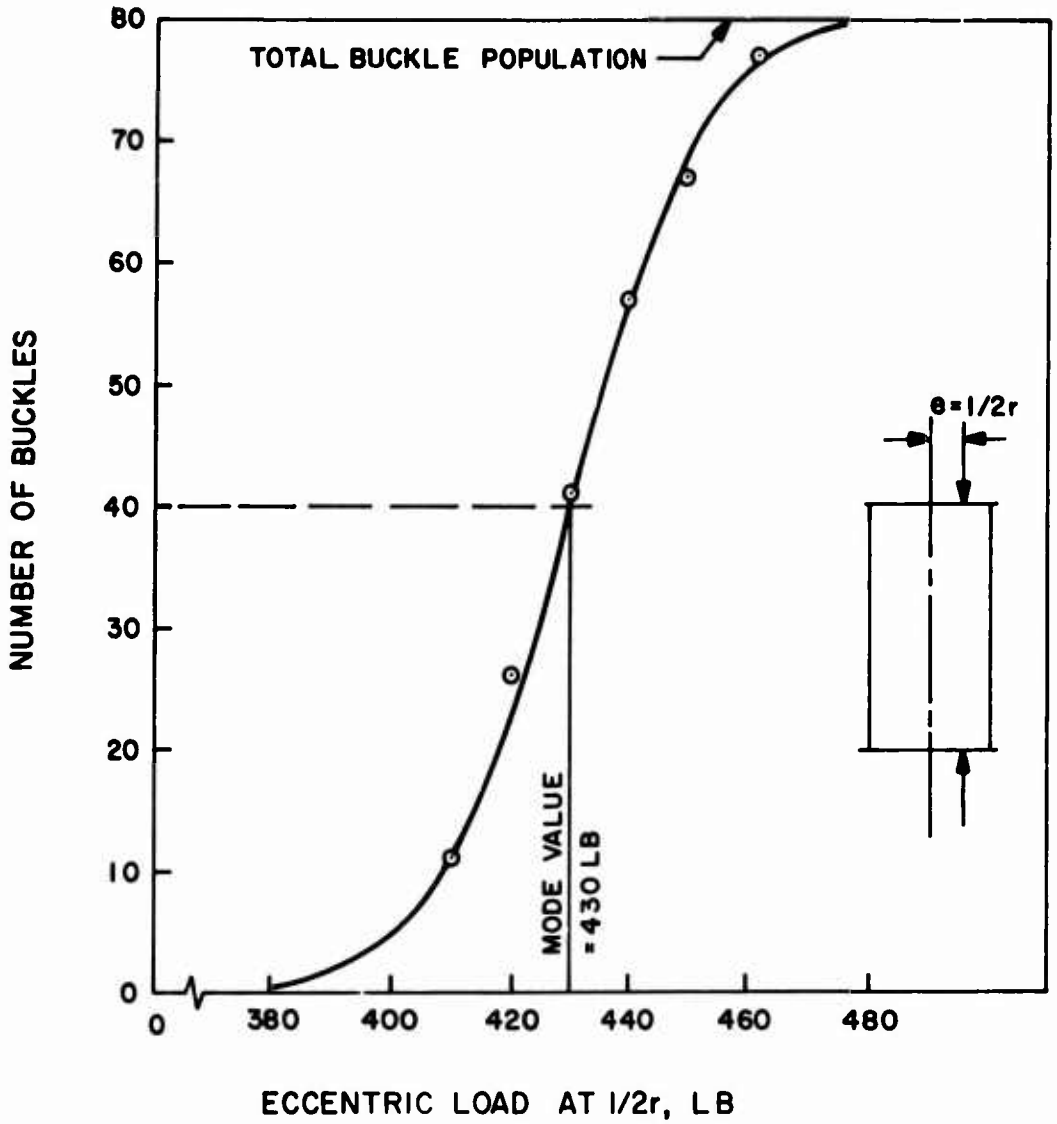

Figure 29. Cumulative Distribution of Buckles as a Function of Load, Shell Specimen of Series 2.

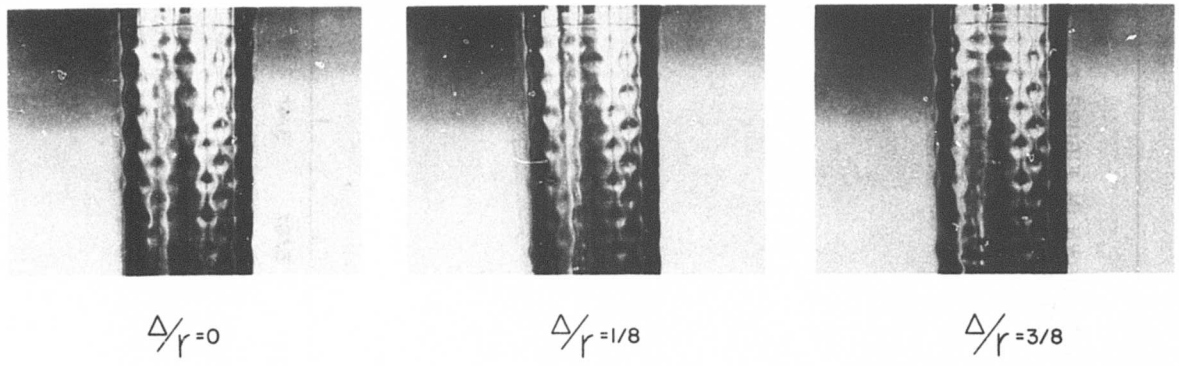

Figure 30. Buckle Patterns for Six Eccentric Load Positions, Series 2 Shell Specimens.

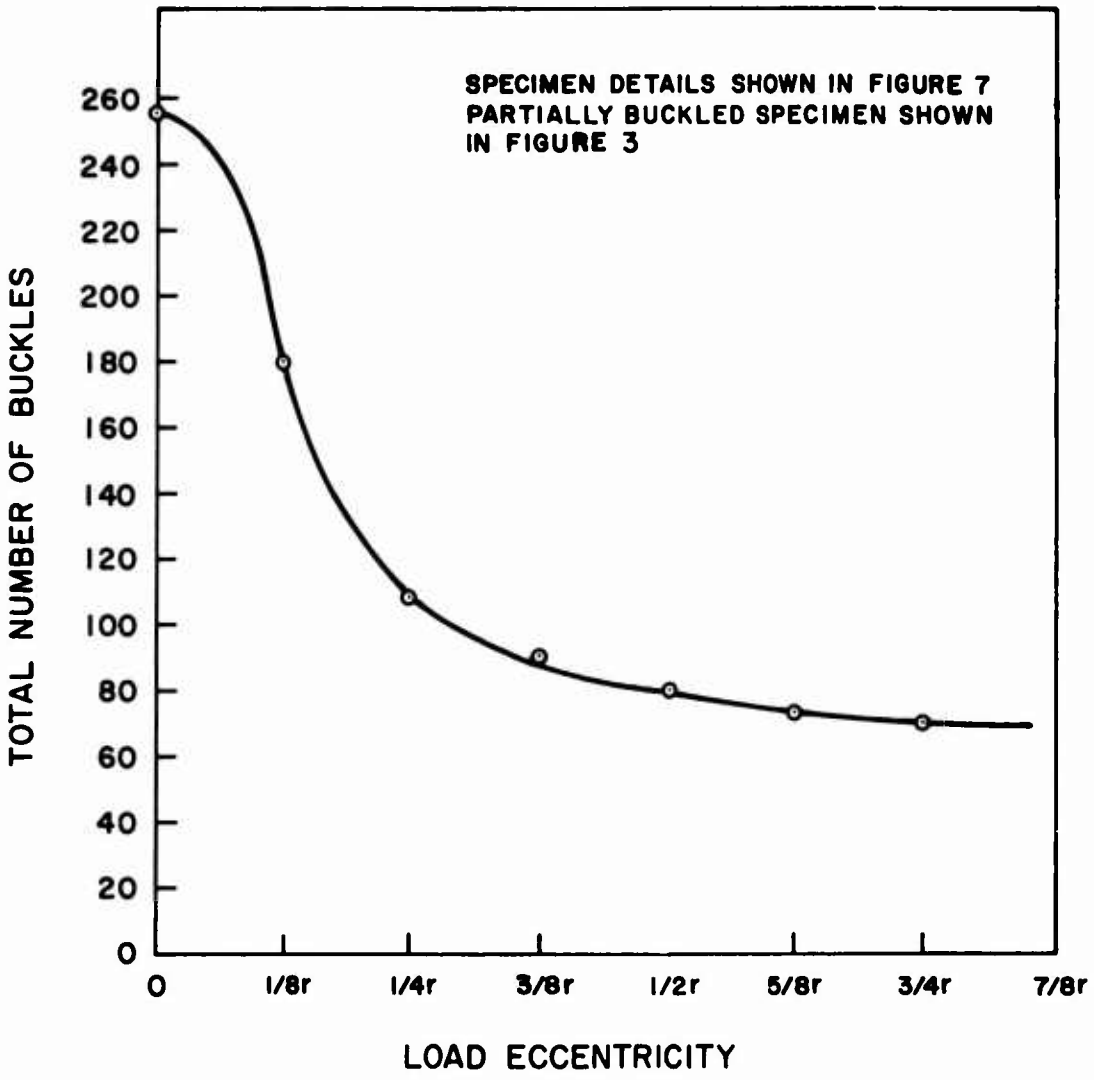

Figure 31. Total Buckle Population as a Function of Load Eccentricity, Shell Specimen of Series 2 Tests.

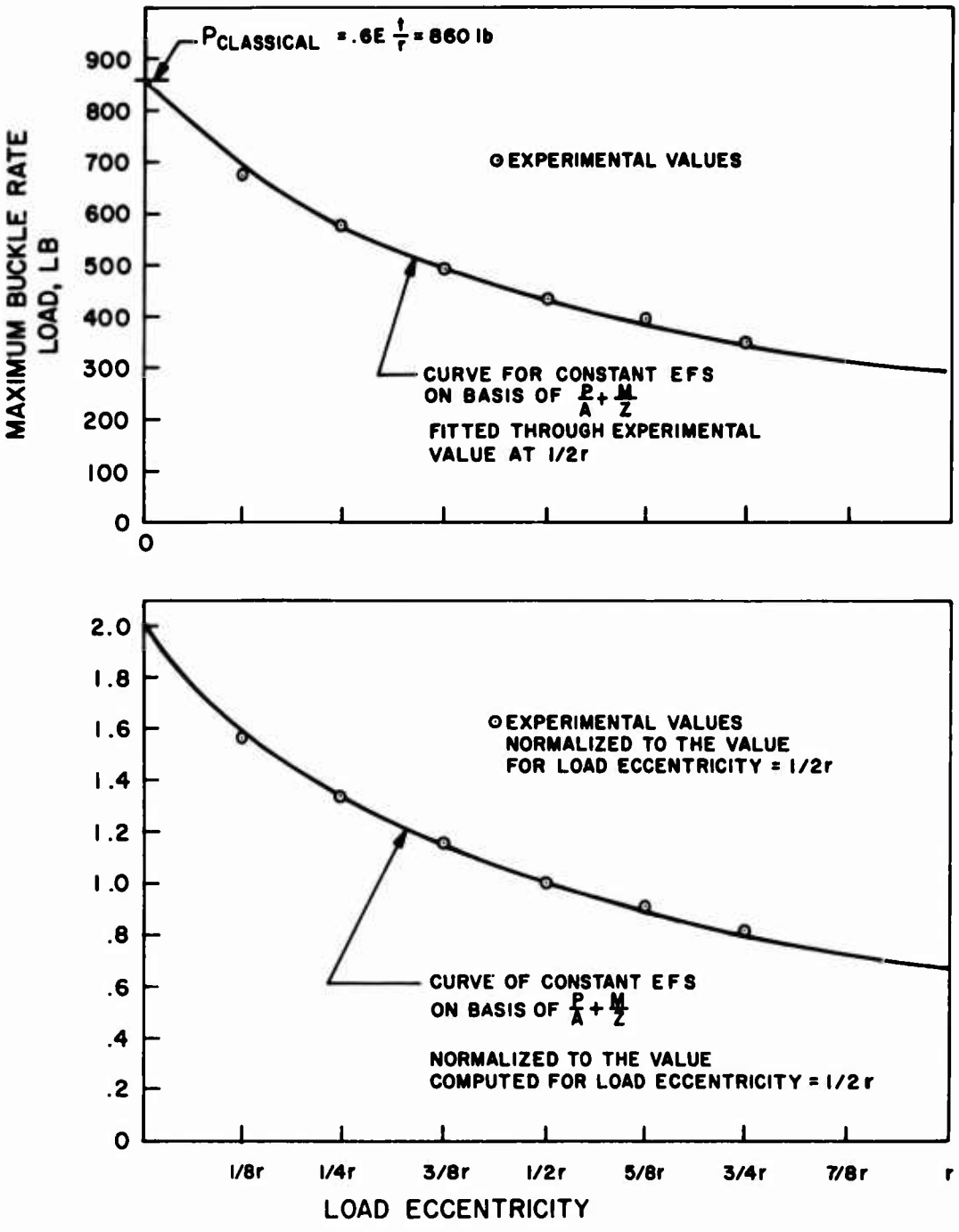

Figure 32. Maximum Buckle Rate Load Versus Load Eccentricity, Shell Specimen of Series 2 Tests.

CONCLUSIONS

The work reported herein is substantial experimental evidence that unstiffened right circular thin-walled cylindrical shells buckle under nonuniform axial load conditions when the maximum compressive stress in the shell reaches the level which would cause instability under uniform load conditions.

It is demonstrated that sound statistical data with regard to shell stability can be as reliably obtained from well-planned tests on single specimens as from a multitude of tests on a wide range of specimens.

A strong indication is given that there is no need to use elaborate methods of fabrication, since incomplete shells may well be as revealing as complete ones.

REFERENCES

1. Flügge, W., DIE STABILITÄT DER KREISZYLINDERSCHALE, Ing.-Archiv, Vol. 3, No. 5, December 1932, pp. 463-506.

2. Timoshenko, S., THEORY OF ELASTIC STABILITY, McGraw-Hill Book Company, Inc., New York, N. Y., 1932, pp. 463-467.

3. Donnell, L. H., A NEW THEORY FOR THE BUCKLING OF THIN CYLINDERS UNDER AXIAL COMPRESSION AND BENDING, Trans. ASME, Vol. 56, 1934, pp. 795-806.

4. Abir, D., and Nardo, S., THERMAL BUCKLING OF CIRCULAR CYLINDRICAL SHELLS UNDER CIRCUMFERENTIAL TEMPERATURE GRADIENTS, Journal of the Aerospace Sciences, Vol. 26, No. 12, December 1959, pp. 803-808.

5. Bijlaard, P., and Gallagher, R., ELASTIC INSTABILITY OF A CYLINDRICAL SHELL UNDER ARBITRARY CIRCUMFERENTIAL VARIATION OF AXIAL STRESS, Journal of the Aerospace Sciences, Vol. 27, No. 11,1960, pp.854-858,866.

6. Seide, P., and Weingarten, V., ON THE BUCKLING OF CIRCULAR CYLINDRICAL SHELLS UNDER PURE BENDING, Journal of Applied Mechanics, ASME, March 1961, pp. 112-116.

7. Lundquist, E., STRENGTH TESTS OF THIN-WALLED DURALUMINUM CYLINDERS IN PURE BENDING, NACA Technical Note No. 479, December 1933.

8. Suer, H., Harris, L., Skene, W., and Benjamin, R., THE BENDING STABILITY OF THIN-WALLED UNSTIFFENED CIRCULAR CYLINDERS INCLUDING THE EFFECTS OF INTERNAL PRESSURE, Journal of the Aeronautical Sciences, Vol. 25, No. 5, May 1958, pp. 281-287.

9. Heise, O., THE EXPERIMENTAL DETERMINATION OF THE BUCKLING LOAD OF AXIAL-COMPRESSED THIN CYLINDRICAL SHELLS, DFL-Report No. 214, German Laboratory of Aero- and Astronautics, 1963.

10. Horton, W., A NEW PHILOSOPHY ON THE BUCKLING OF SHELL BODIES, (report in preparation).

11. Wilson, E., AN INTRODUCTION TO SCIENTIFIC RESEARCH, McGraw-Hill Book Company, Inc., New York, N. Y., 1952.

12. Mossakovskii, V. I., and Smelyi, G. N., EXPERIMENTAL INVESTIGATION OF THE INFLUENCE OF RIGIDITY OF THE TESTING MACHINE ON THE STABILITY OF CYLINDRICAL UNREINFORCED SHELLS UNDER AXIAL COMPRESSION, Izv. AN SSR, OTN, Mekh. i Mashino, No. 4, 1963, pp. 162-166.

13. Bowker, A. H., and Lieberman, G. J., ENGINEERING STATISTICS, Prentice-Hall, Inc.,1959 , Chapter IX and Tables 3 and 4.

APPENDIX
STATISTICAL TREATMENT OF THE RESULTS OF THE FIRST SERIES OF TESTS

The data obtained from buckling tests of 349 cylindrical shell specimens are contained in Tables I through V. These tests are described in detail in the body of the report, and the test data are interpreted graphically in Figures 19 and 20. The data of Figure 19 pertain to loading distributions designated Type A, while those of Figure 20 represent the results from loading distributions designated Type B. The purpose of this appendix is to present the results of a statistical analysis which was performed on the data of these two figures.

An underlying physical relationship relating the fraction of cylinder end perimeter loaded to a corresponding value of buckling load is unknown. It is true that the work of Bijlaard and Gallagher, discussed in the Introduction to this report and described in detail in Reference 5, provides a theoretical basis for predicting such a physical relationship. However, valid theoretical work covering the range of loading distributions of interest in this study could not be found. Thus, the statistical problem before us is to determine in terms of confidence levels the degree of association which exists between the fraction of perimeter loaded and the buckling load.

The procedures followed are those outlined in the text by Bowker and Lieberman.[13] Similar procedures are available in most modern references on experimental statistics, a notable example being Handbook 91 of the National Bureau of Standards. A confidence level of 95 percent was chosen in all the work presented here.

BUCKLING DATA FROM TYPE A LOADING

These are the results shown graphically in Figure 19. The general appearance of the plot indicates a high degree of linear association between the fraction of perimeter loaded and the buckling load. Also, it appears that a single line representation of the data would pass through the origin.

It is not surprising that the latter tendency should appear. An examination of details of the Type A load distribution described in Figures 10, 11, and 12 shows that the magnitude of load required to produce a given level of stress in the shell wall approaches zero as the fraction of perimeter loaded approaches zero.

All numerical quantities from the experimental data required in the analyses presented here are found in Table IX.

Test for Linearity

At four values for the fraction of perimeter loaded, more than one mean value of buckling load was observed. Thus, we may analyze the data for linearity using an F test.

Hypothesis: the association between the variables is linear.
Rejection Criterion:

TABLE IX. TREATMENT OF EXPERIMENTAL DATA GIVEN IN FIGURE 19

i	f_i	f_i^2	P_{i1}	P_{i2}	P_{i3}	$\bar{P}_i$	$f_i\bar{P}_i$	$(f_i-\bar{f})$	$(f_i-\bar{f})^2$	$(\bar{P}_i-\bar{\bar{P}})$	$\frac{(f_i-\bar{f})}{(P_i-\bar{\bar{P}})}$	$\tilde{P}_i$	$(\bar{P}_i-\tilde{P}_i)$	$(P_i-\tilde{P}_i)^2$	$(P_{i1}-\bar{P}_i)$	$(P_{i1}-\bar{P}_i)^2$	$(P_{i2}-\bar{P}_i)$	$(P_{i2}-\bar{P}_i)^2$	$(P_{i3}-\bar{P}_i)$	$(P_{i3}-\bar{P}_i)^2$
1	.05	.0025	150	-	-	150	8	-.495	.245	-908	450	178	-28	784	0	0	-	-	-	-
2	.25	.0625	520	-	-	520	130	-.295	.087	-538	159	535	-15	225	0	0	-	-	-	-
3	.33	.1090	620	860	-	740	244	-.215	.046	-318	68	675	65	4225	-120	14400	120	14400	-	-
4	.50	.2500	870	1020	1040	980	490	-.045	.002	- 78	3	978	2	4	-110	12100	40	1600	60	3600
5	.67	.4500	1130	1210	-	1200	805	.125	.016	143	18	1280	80	6400	- 20	400	10	100	-	-
6	.71	.5050	1420	-	-	1420	1010	.165	.028	363	60	1350	70	4900	0	0	-	-	-	-
7	.85	.7220	1570	1620	-	1590	1352	.350	.093	533	162	1600	-10	100	- 20	400	30	900	-	-
8	1.00	1.0000	1860	-	-	1860	1860	.455	.207	803	365	1865	- 5	25	0	0	-	-	-	-
$\sum$	4.36					8460	5899		.724		1285			16663		27300		17000		3600

$$\bar{f} = \frac{1}{n}\sum_{i=1}^{8} f_i = \frac{4.36}{8} = .545$$

$$\bar{\bar{P}} = \frac{1}{n}\sum_{i=1}^{8} \bar{P}_i = \frac{8460}{8} = 1058 \text{ lb}$$

$\tilde{P}_i = 88 + 1780F$

(see Test for Zero Intercept Section)

f = Independent variable designating fraction of perimeter loaded, dimensionless
P = Dependent variable designating buckling load, pounds of force
P_{ij} = A jth value of buckling load observed to correspond to the ith value of f
n = Number of values of i = 8
k = Number of values of j = $\frac{1+1+2+3+2+1+2+1}{8} \sim 2$, an estimated average number of observations of P for each chosen value of f.

$$F = \frac{k \sum_{i=1}^{n} (\bar{P}_i - \tilde{P}_i)^2}{n - 2} + \frac{\sum_{i=1}^{n} \sum_{j=1}^{k} (P_{ij} - \bar{P}_i)}{n(k - 1)} \qquad (4)$$

$\geq F_{\alpha; n-2,\ n(k-1)}$ = the 100α percentage point of the F distribution with degrees of freedom $n - 2$ and $n(k - 1)$. $\alpha = .05$ at 95-percent confidence level.

When values are taken from Table IX to compute F,

$$F = 2. \frac{16,663}{6} + \frac{47,900}{8} = .922 \qquad (5)$$

$$F_{.05;\ 6,8} = 3.58$$

$.922 < 3.58$ and the hypothesis of linearity is not rejected at the 95-percent level.

Test for Zero Intercept

Having accepted the hypothesis of linear association, we now proceed to fit a straight line to the data points. For this purpose we use the method of least squares.

$$\tilde{P} = a + bf \qquad (6)$$

a = vertical axis intercept
b = slope

$$b = \sum_{i=1}^{n} (f_i - \bar{f})(\bar{P}_i - \bar{\bar{P}}) + \sum_{i=1}^{n} (f_i - \bar{f})^2$$

$$= \frac{1285}{.724} = 1780 \text{ lb}$$

$$a = \bar{\bar{P}} - b\bar{f} = 1058 - 1780 \times .545 = 88 \text{ lbs}$$

Thus, $\tilde{P} = 88 + 1780f$ is a least-squares linear representation of the association between the variables.

In view of the physical requirement described above, that such a linear representation must extend through the origin as a limit, it would appear that

the value of 88 pounds indicated experimentally for the vertical axis intercept is accidental. We now test for this occurrence using a Student "t" test.

Hypothesis: $a = 0$
Rejection Criterion:

$$\left| \frac{a}{s_{pf}\sqrt{\frac{1}{n} + \frac{\bar{f}^2}{\sum_{i=1}^{n}(f_i - \bar{f})^2}}} \right| \geq t_{\alpha/2;n-2} \qquad (7)$$

where

$$s_{Pf} = \sqrt{\frac{\sum_{i=1}^{n}(\bar{P}_i - \tilde{P}_i)^2}{n-2}} = \sqrt{\frac{16,663}{6}} = 53 \text{ lb}$$

$t_{\alpha/2;n-2}$ = the $100\alpha/2$ percentage point of the "t" distribution with degrees of freedom $n - 2$

$$= t_{.025;6} = 2.447$$

$$\sqrt{\frac{1}{n} + \frac{\bar{f}^2}{\sum_{i=1}^{n}(f_i - \bar{f})^2}} = \sqrt{\frac{1}{8} + \frac{.545^2}{.724}} = .731$$

$$\left| \frac{88}{53 \times .731} \right| = 2.27 < 2.447$$

and the hypothesis that $a = 0$ is not rejected at the 95-percent level.

Straight-Line Fit With Zero Intercept

Accepting the hypothesis of linearity and zero intercept on the vertical axis, we now fit a least-squares line through the experimental points which extend through the origin.

$$\tilde{P} = bf \tag{8}$$

$$b = \sum_{i=1}^{n} f_i \bar{P}_i \div \sum_{i=1}^{n} f_i^2 = \frac{5899}{3.1010} = 1890$$

$$\tilde{P} = 1890f$$

This is the line shown in Figure 19 and is considered to be the best statistical representation of these experimental data.

Confidence Interval Estimate of Slope

As a final analysis of the data of Figure 10, a 95-percent confidence interval estimate for the slope b computed in Equation (8) will be made. We assume no a priori knowledge of values for standard deviation of the values of P_{ij}; therefore, we base the estimate on a Student "t" distribution.

$$\text{Interval} = b \pm t_{\alpha/2;n-1} \frac{s_{Pf}}{\sqrt{\sum_{i=1}^{n} f_i^2}} \tag{9}$$

$$s_{Pf} = \sqrt{\frac{\sum_{i=1}^{n} (\bar{P}_i - \tilde{P}_i)^2}{n-1}} = \sqrt{\frac{16,663}{7}} = 49 \text{ lb}$$

$$\sqrt{\sum_{i=1}^{n} f_i^2} = \sqrt{3.1010} = 1.76$$

$$t_{\alpha\ 2;n-1} = t_{.025;7} = 2.365$$

$$\text{Interval} = 1890 \pm 2.365 \times \frac{49}{1.76}$$

$$= 1890 \pm 66 \text{ lb}$$

$$[1824, 1956 \text{ lb}]$$

Summarizing Statement

As a result of the foregoing treatment of the data of Figure 19, the following statement can be made. With probability .95, the true experimental relationship between fraction of perimeter loaded and buckling load for Type A loading is contained within the bounds of the two lines $P = 1824f$ and $P = 1956f$.

BUCKLING DATA FROM TYPE B LOADING

These results are shown graphically in Figure 20. As was the case for Type A loading, a high degree of linear association between fraction of perimeter loaded and buckling load is indicated by the plot. However, in this case it is clear that a single line representation of the data would not pass through the origin. Rather, for zero fraction of perimeter loaded, a relatively high value of loading is apparently required to cause buckling.

To explain the latter observation, we again appeal to an examination of the physical details of how an external load is transmitted to the edge of the shell. Figures 13 and 14 show the Type B loading, while the manner in which the continuous rims participate in load transfer to the shell is described in the body of the report. It is clear for Type B loading that as the fraction of loaded rims perimeter approaches zero, the fraction of shell perimeter reacting this load approaches a limiting value greater than zero. This is due tc the bending stiffness of the rims.

In the case of a concentrated load on the end rim, representing zero fraction of perimeter loaded, the shell load is distributed along a finite length of the perimeter. An estimate of this limiting case was computed by treating the end rim as a beam on an elastic foundation. This computed value was then used to estimate the vertical axis intercepts shown in Figure 20.

All numerical quantities from the experimental data required in the following analyses are found in Table X.

Straight-Line Fit

Acceptance of linearity for the association between variables is based on the analysis performed for Type A loading, together with the general appearance of the plot in Figure 20.

The rim analysis described above indicates that for values of f greater than .15, the degree to which rim stiffness participates in load transfer to the shell rim diminishes rapidly. Thus, a straight-line fit will be regarded as significant only for values of f greater than .15.

TABLE X. TREATMENT OF EXPERIMENTAL DATA GIVEN IN FIGURE 20

i	f_i	P_i	$(f_i-\bar{f})$	$(P_i-\bar{P})$	$(f_i-\bar{f})^2$	$(f_i-\bar{f})(P_i-\bar{P})$	$\tilde{P}_i$	$(P_i-\tilde{P}_i)$	$(P_i-\tilde{P}_i)^2$
1	.15	590	-.40	-620	.1600	248	570	20	400
2	.25	740	-.30	-470	.0900	141	730	10	100
3	.33	930	-.22	-280	.0484	62	863	67	4500
4	.49	1070	-.06	-140	.0036	8	1115	-45	2030
5	.50	1110	-.05	-100	.0025	5	1130	-20	400
6	.67	1300	-.12	90	.0144	11	1396	-96	9220
7	.71	1590	-.16	380	.0256	61	1467	123	15120
8	.85	1690	-.30	480	.0900	144	1690	0	0
9	1.00	1860	-.45	750	.2025	338	1930	70	4900
$\sum$	4.95	10880			.6370	1018			36670

$n = 9$

$$\bar{f} = \frac{1}{n}\sum_{i=1}^{9} f_i = \frac{4.95}{9} = .550$$

$$\bar{P} = \frac{1}{n}\sum_{i=1}^{9} P_i = \frac{10880}{9} = 1210 \text{ lb}$$

$\tilde{P} = 330 + 1600f$
(see Straight-Line Fit section)

f = Independent variable designating fraction of perimeter loaded, dimensionless
P = Dependent variable designating buckling load, pounds of force
P_i = The value of buckling load observed to correspond to the i^{th} value of f

$$b = \sum_{i=1}^{n} (f_i - \bar{f})(P_i - \bar{P}) + \sum_{i=1}^{n} (f_i - \bar{f})^2$$

$$= \frac{1018}{.637} = 1600 \text{ lb}$$

$$a = \bar{P} - b\bar{f} = 1210 - 1600 \times .550$$

$$= 330 \text{ lb}$$

$$\tilde{P} = 330 + 1600f \tag{10}$$

Confidence Intervals for P

A confidence interval estimate for values of P for a given value of f will be computed. Again, the estimate will be based on the Student "t" distribution.

$$\text{Interval} = \tilde{P} \pm t_{\alpha/2;n-2} \cdot s_{Pf} \sqrt{\frac{1}{n} + \frac{(f - \bar{f})^2}{\sum_{i=1}^{n} (f_i - \bar{f})^2}} \tag{11}$$

$$s_{Pf} = \sqrt{\frac{\sum_{i=1}^{n} (P_i - \tilde{P})^2}{n - 2}} = \sqrt{\frac{36,670}{7}} = 73 \text{lb}$$

$$t_{\alpha/2;n-2} = t_{.025;7} = 2.365$$

$$\sqrt{\frac{1}{n} + \frac{(f - \bar{f})^2}{\sum_{i=1}^{n} (f_i - \bar{f})^2}} = \sqrt{\frac{1}{9} + \frac{(f - \bar{f})^2}{.637}}$$

$$= \frac{1}{3} \sqrt{1 + 1.413(F - .55)^2}$$

$$\text{Interval} = \tilde{P} \pm 57\sqrt{1 + 1.413(f - .55)^2},\ f > .15 \qquad (12)$$

at the 95-percent confidence level.

Three sample values:

f	P	$57\sqrt{1 + 1.413(f-.55)^2}$	Interval
.15	570	63 lb	[507,633]
.55	1210	57	[1153,1267]
1.00	1930	65	[1865,1995]

Summarizing Statement

As a result of the above treatment of the data of Figure 20, the following statement can be made for values of f greater than .15. With probability .95, the true experimental relationship between fraction of perimeter loaded and buckling load for Type B loading is contained within the interval

$$\tilde{P} \pm 57\sqrt{1 + 1.413(f - .55)^2},\ f > .15 \qquad (13)$$

$$\tilde{P} = 330 + 1600f$$